Gravity, Magnetics, and Geology of the San Andreas Fault Area Near Cholame, California

GEOLOGICAL SURVEY PROFESSIONAL PAPER 646-C

Gravity, Magnetics, and Geology of the San Andreas Fault Area Near Cholame, California

By W. F. HANNA, S. H. BURCH, *and* T. W. DIBBLEE, JR.

GEOPHYSICAL FIELD INVESTIGATIONS

GEOLOGICAL SURVEY PROFESSIONAL PAPER 646-C

UNITED STATES GOVERNMENT PRINTING OFFICE, WASHINGTON: 1972

UNITED STATES DEPARTMENT OF THE INTERIOR

ROGERS C. B. MORTON, *Secretary*

GEOLOGICAL SURVEY

V. E. McKelvey, *Director*

Library of Congress catalog-card No. 72-600080

For sale by the Superintendent of Documents, U.S. Government Printing Office
Washington, D.C. 20402 Stock Number 2401-2170

CONTENTS

	Page
Abstract	C1
Introduction	1
Methods of investigation	2
Gravity survey	2
Gravity interpretation	7
Magnetic surveys	8
Magnetic interpretation	8
Geologic setting	8
Rock units	9
Plutonic and metamorphic rocks	9
Ultramafic rocks	9
Franciscan rocks	11
Cretaceous and Eocene miogeosynclinal rocks	11
Middle and upper Tertiary rocks	12
Distribution	12
Volcanic rocks	12
Lower Miocene sedimentary rocks	12
Monterey Shale	12
Upper Miocene and Pliocene sedimentary rocks	13
Upper Cenozoic valley deposits	13
Rock units—Continued	
Surficial deposits	C13
Geologic structure and tectonics	13
Structural setting	13
Structural history	14
Diablo Range	15
Parkfield-Turkey Flat area	15
Temblor Range	15
Gold Hill area	15
Southwest of San Andreas fault	16
Gravity and magnetic features	16
General patterns	16
Gravity trends	16
Magnetic trends	16
Anomalies northeast of San Andreas fault	16
Gravity high at Cholame Valley	16
Anomalies at Table Mountain	17
Magnetic high at Palo Prieto Pass	20
Other gravity features	25
Gravity anomalies southwest of San Andreas fault	25
Summary	27
References	27

ILLUSTRATIONS

[Plates 1–4 are in pocket]

PLATE 1. Complete Bouguer gravity and generalized geologic map along the San Andreas fault near Cholame, Calif.
2. Aeromagnetic and generalized geologic map along the San Andreas fault near Cholame.
3. Vertical-intensity ground magnetic and generalized geologic map along the San Andreas fault near Cholame.
4. Idealized cross sections, gravity profiles, and magnetic profiles across the San Andreas fault near Cholame.

	Page
FIGURE 1. Index map showing area investigated	C2
2. Comparison of computed gravity anomaly of model with observed anomaly near Cholame Valley	17
3. Comparison of computed magnetic and gravity anomalies of models with observed anomalies at Table Mountain	18
4. Comparison of computed total-intensity magnetic anomalies of models with observed aeromagnetic anomaly at Palo Prieto Pass	20
5. Comparison of computed total-intensity and vertical-intensity magnetic anomalies of models with observed aeromagnetic and ground magnetic anomalies at Palo Prieto Pass	23
6. Map showing sampling sites	24
7. Comparison of computed magnetic and gravity anomalies of a model with observed anomalies at Palo Prieto Pass	26

TABLES

	Page
TABLE 1. Principal facts for gravity bases	C2
2. Principal facts for gravity stations	3
3. Selected exploratory wells	10
4. Summary of magnetic susceptibility data	24

GEOPHYSICAL FIELD INVESTIGATIONS

GRAVITY, MAGNETICS, AND GEOLOGY OF THE SAN ANDREAS FAULT AREA NEAR CHOLAME, CALIFORNIA

By W. F. HANNA, S. H. BURCH, and T. W. DIBBLEE, JR.

ABSTRACT

Complete Bouguer gravity, aeromagnetic, and ground magnetic data interpreted in light of geologic mapping and well data within a 30-minute quadrangle centered near Cholame, Calif., express highly contrasting subsurface rock and structural patterns on opposite sides of the San Andreas fault.

The geologic terrane northeast of the fault is composed of pervasively sheared Franciscan sedimentary and volcanic rocks of Mesozoic age and ultramafic rocks overlain by a thick series of severely deformed Cretaceous and Tertiary sedimentary rocks and locally deformed Quaternary valley sediments. The terrane southwest of the fault has a basement of Mesozoic plutonic and metamorphic rocks overlain by gently folded Tertiary sedimentary rocks and Quaternary valley sediments.

Northeast of the San Andreas fault the geophysical data reveal the presence of (1) a major gravity high between Parkfield and Cholame, associated with relatively dense, nonmagnetic Franciscan and Cretaceous miogeosynclinal rocks overlain by Cenozoic rocks in the northeastern Diablo Range and in contact with low-density Cenozoic rocks southwest of the fault, (2) an elongate magnetic ridge and gravity trough at Table Mountain, probably generated by a thick tabular body of serpentinite dipping steeply north-northeast, inferred to be the main source of the serpentinite extrusion along this mountain, (3) a major elliptical magnetic high in an area of low density gradient near Palo Prieto Pass, probably associated with a large, deeply buried serpentine-rich body bounded on the southwest by the vertical San Andreas fault and on the northeast by a northeast-dipping contact or fault with nonmagnetic rocks, and (4) a northwest-trending gravity low over the Kettleman Plain, probably produced by a thickening of low-density Cenozoic sedimentary rocks near the axis of a major syncline.

Southwest of the San Andreas fault the data show (1) a local gravity high north of Red Hills, associated with an uplift of plutonic and metamorphic rocks in these hills on the northeast side of the San Juan fault, (2) a prominent southwest-sloping northwest-trending gravity gradient southeast of Red Hills, which suggests a buried basement fault or a steep subsurface contact between basement and sedimentary rocks extending from the San Juan fault southeastward to the San Andreas fault near the southern end of the quadrangle, (3) a discontinuous northwest-trending gravity trough east and north of Shandon, probably associated with a depression of the basement surface under an area near San Juan Creek, and (4) a broad northeast-trending gravity plateau west-southwest of Shandon, probably associated with a thinning of Cenozoic sedimentary rocks overlying a shallow basement surface that slopes from the extensive basement exposures of the La Panza Range southwest of the quadrangle.

INTRODUCTION

This report considers the relationship of Bouguer gravity data, total-intensity aeromagnetic data, and vertical-intensity ground magnetic data to generalized geology in an area critical to an understanding of the San Andreas fault. The gravity data are presented as a 2-mgal (milligal) complete Bouguer anomaly map overprinted on the geologic map. These data were collected by S. H. Burch as part of a regional survey for the San Luis Obispo 1:250,000 sheet (Burch and others, 1971). The magnetic data include a 20-gamma reconnaissance aeromagnetic map supported in much of the area by ground magnetic coverage. These data are part of a broader study of the San Andreas fault by Hanna and others (1972). The geology was mapped by T. W. Dibblee as part of a regional geologic mapping project of the southern Coast Ranges adjacent to and near the San Andreas fault. Detailed geologic mapping by Dickinson (1966a, 1966b) of part of the area of this report was incorporated.

The mapped area, centered near Cholame, Calif. (fig. 1), contains a 42-mile section of the San Andreas fault. It is a 30- by 30-minute block covering nearly 1,000 square miles in the southern Coast Ranges. It is composed of the Orchard Peak, Parkfield, "Reef Ridge," and Shandon 15-minute quadrangles. "Reef Ridge" is the name here applied to the unpublished 15-minute quadrangle containing

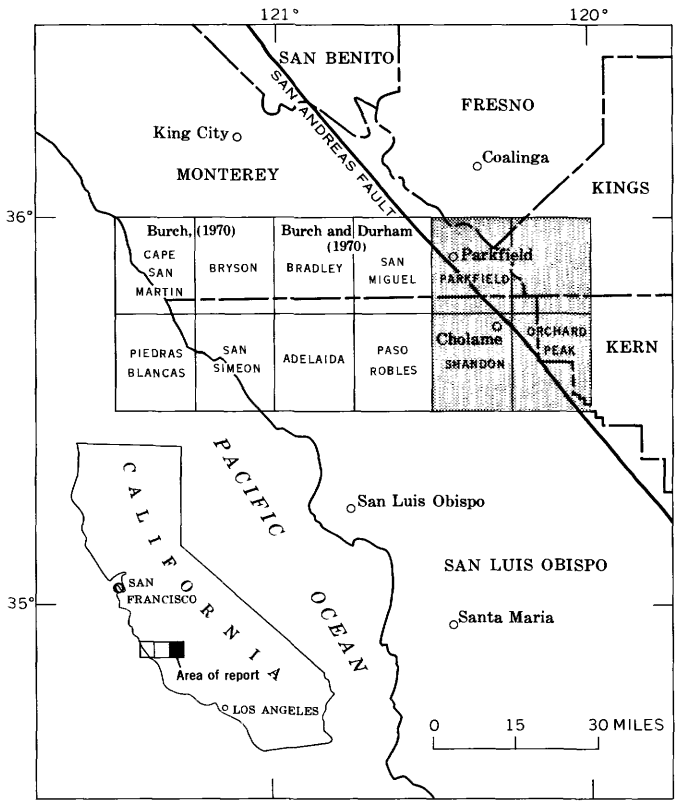

FIGURE 1.—Map showing area investigated.

the Garza Peak, Kettleman Plain, Pyramid Hills, and Tent Hills 7½-minute quadrangles.

The authors are indebted to Holly C. Wagner, U.S. Geological Survey, who provided data from exploratory wells essential for much of the subsurface interpretation. We also benefited from discussions with R. D. Brown, Andrew Griscom, D. C. Ross, R. G. Coleman, M. C. Blake, and Ivan Barnes, of the U.S. Geological Survey, and with Professor B. M. Page of Stanford University.

METHODS OF INVESTIGATION

GRAVITY SURVEY

The map area includes 268 gravity stations tied to 11 base stations. Principal facts for the base stations are listed in table 1; those for all other stations, in table 2. The data are referenced to California Division of Mines and Geology Base Station 173 (Chapman, 1966, p. 36) at the U.S. Geological Survey headquarters in Menlo Park, Calif. The observed gravity at this base, determined by numerous ties to the North American Gravity Standardization Stations at the San Francisco International Airport, is taken to be 979,958.74 mgal.

The precision of the gravity data varies from station to station. The observed gravity measurements for the 219 stations read with LaCoste-Romberg gravity meters have a precision of about 0.03 mgal after correcting for lunar and solar tidal effects. Observed gravity values of the 49 stations read with a Worden gravity meter (scale constant about 0.5 mgal per scale division) have a precision of about 0.1 to 0.2 mgal after correcting for instrument drift. Latitude and longitude were measured to within 0.02 minute by using Geological Survey topographic maps. Elevation accuracies vary considerably according to the types of source data. Roughly 60 percent of the stations were read on or near bench marks where elevations are precise to at least 0.5 feet. Another 20 percent are field-checked spot elevations precise to about 2 feet, and 20 percent are unchecked photogrammetric elevations precise to about 5 or 10 feet, depending on the map contour interval. Three elevations were established by altimetry with an estimated precision of 10 to 20 feet.

All gravity data were corrected for terrain effects (by using the standard density 2.67 g/cm^3) to a distance of 166.7 km (kilometer) from the gravity station. For the inner zones (within 2.29 km of the

TABLE 1.—*Principal facts for bases used in gravity survey*

[Observed gravity: The amount of scatter among numerous ties between these bases suggests that the relative gravity of each is known to be ±0.02 milligals. Description: USC&GS, U.S. Coast and Geodetic Survey; USGS, U.S. Geological Survey; BM, bench mark]

Base	Latitude N.	Longitude W.	Elevation (ft)	Observed gravity	Description
SLUKB	36° 7.73′	121° 1.12′	405.8	979,793.04	USC&GS BM G154 at San Lucas.
BRADB	35° 51.81′	120° 47.73′	552.0	979,737.30	USGS BM 553 at Bradley.
PSROB	35° 37.55′	120° 41.28′	720.0	979,717.17	USC&GS BM L24 at Paso Robles.
BLAKB	35° 36.92′	119° 52.01′	643.2	979,675.00	USC&GS BM R11 at Blackwell's corner.
CLNGB	36° 8.73′	120° 21.18′	667.0	979,740.39	USC&GS BM J156 at Coalinga.
AVNLB	35° 59.54′	120° 7.65′	754.0	979,714.30	USC&GS BM W11 at Avenal.
PARKB	35° 53.98′	120° 25.92′	1,535.0	979,687.69	USC&GS BM F79 at Parkfield.
SHANB	35° 39.33′	120° 22.71′	1,038.0	979,686.02	USC&GS BM W559 at Shandon.
CHLMB	35° 44.05′	120° 17.26′	1,137.0	979,699.65	USC&GS BM A624 at Cholame.
CRZOB	35° 33.44′	120° 6.38′	1,664.0	979,644.84	USC&GS BM J616 in sec. 23, T. 27 S., R. 17 E.
KECKB	35° 40.27′	120° 4.85′	845.0	979,713.49	USC&GS BM N559 at Kecks Corner.

TABLE 2.—*Principal facts for gravity stations*

[Gravity data is in milligal]

Station	Latitude N.		Longitude W.		Elevation (ft)	Observed gravity	Terrain correction	Free air anomaly	Complete Bouguer anomaly
	Deg	Min	Deg	Min					
622	35	35.40	120	28.88	1,353.0	979,666.62	0.93	−1.82	−47.58
623	35	35.27	120	27.23	1,407.0	979,662.22	.75	−.96	−48.76
649	35	59.82	120	28.21	3,506.0	979,564.67	7.93	63.88	−48.93
650	35	58.81	120	27.22	2,749.0	979,612.84	3.39	42.31	−49.04
651	35	39.54	120	29.21	976.0	979,691.53	.64	−18.26	−51.31
652	35	39.55	120	27.00	973.0	979,695.84	.72	−14.24	−47.11
653	35	39.54	120	24.75	1,000.0	979,692.41	.69	−15.12	−48.95
SHANB	35	39.33	120	22.71	1,038.0	979,686.00	.65	−17.66	−52.84
655	35	40.39	120	20.97	1,073.0	979,683.20	1.03	−18.67	−54.68
656	35	41.98	120	19.39	1,102.0	979,690.53	1.06	−10.88	−47.86
657	35	42.86	120	18.27	1,164.0	979,689.89	.98	−6.94	−46.14
CHLMB	35	44.05	120	17.26	1,137.0	979,699.68	.77	−1.39	−39.86
659	35	44.27	120	15.85	1,243.0	979,700.64	.87	9.23	−32.80
660	35	44.50	120	13.98	1,677.0	979,673.41	.99	22.49	−34.37
661	35	44.01	120	12.43	1,518.0	979,682.95	1.37	17.77	−33.23
662	35	43.16	120	10.71	1,308.0	979,695.56	2.04	11.84	−31.26
663	35	42.13	120	8.81	1,097.0	979,701.43	1.33	−.66	−37.20
664	35	41.23	120	6.88	917.0	979,710.31	.86	−7.43	−38.23
KECKB	35	40.27	120	4.85	845.0	979,713.95	.54	−9.20	−37.83
666	35	39.22	120	2.67	745.0	979,715.57	.52	−15.49	−40.69
667	35	38.09	120	.36	746.0	979,699.09	.39	−30.27	−55.64
669	35	41.49	120	3.38	750.0	979,720.83	.40	−12.99	−38.49
670	35	42.40	120	2.25	722.0	979,723.08	.35	−14.67	−39.25
671	35	43.63	120	.92	662.0	979,721.55	.36	−23.60	−46.10
672	35	45.55	120	18.28	1,142.0	979,700.05	.73	−2.68	−41.37
673	35	46.71	120	19.74	1,154.0	979,704.45	.84	1.19	−37.80
674	35	48.35	120	21.27	1,202.0	979,705.05	.81	3.97	−36.71
675	35	49.11	120	22.72	1,266.0	979,700.96	1.02	4.81	−37.86
676	35	50.79	120	22.72	1,309.0	979,705.51	1.06	11.01	−33.10
677	35	52.45	120	24.71	1,449.0	979,693.71	1.16	10.01	−38.83
PARKB	35	53.98	120	25.92	1,535.0	979,687.56	1.23	9.76	−41.97
722	35	37.81	120	23.93	1,146.0	979,680.19	.54	−11.15	−50.16
723	35	35.11	120	25.59	1,159.0	979,677.77	.77	−8.50	−47.74
724	35	33.38	120	28.44	1,533.0	979,652.15	1.04	2.80	−49.05
725	35	32.94	120	29.52	1,173.0	979,676.27	.79	−5.60	−45.30
726	35	31.36	120	29.65	1,150.0	979,678.31	.75	−3.48	−42.42
727	35	30.13	120	28.19	1,318.0	979,665.45	.87	1.21	−43.40
728	35	31.89	120	26.90	1,268.0	979,666.21	.84	−5.23	−48.15
729	35	30.58	120	26.03	1,536.0	979,651.70	1.14	7.32	−44.53
730	35	31.84	120	24.20	1,277.0	979,662.51	.78	−8.02	−51.31
731	35	30.75	120	23.82	1,323.0	979,659.76	.82	−4.89	−49.73
732	35	33.34	120	24.81	1,252.0	979,666.05	.86	−8.96	−51.31
733	35	36.91	120	26.08	1,063.0	979,686.62	.78	−11.24	−47.16
734	35	36.74	120	28.46	1,441.0	979,660.36	.95	−1.71	−50.48
735	35	38.04	120	28.95	908.0	979,696.57	1.05	−17.48	−47.78
736	35	42.46	120	22.63	1,428.0	979,665.60	1.03	−5.83	−54.08
737	35	41.27	120	23.39	1,241.0	979,675.54	1.09	−11.79	−53.53
738	35	44.00	120	24.09	1,760.0	979,647.43	.98	5.03	−54.70
739	35	44.53	120	25.54	1,864.0	979,640.60	1.55	7.22	−55.52
740	35	43.03	120	25.53	1,426.0	979,666.64	.95	−5.79	−54.05
741	35	41.79	120	26.08	1,462.0	979,662.66	1.21	−4.62	−53.86
742	35	41.49	120	28.14	1,356.0	979,668.91	1.29	−7.91	−53.42
743	35	40.90	120	29.45	1,252.0	979,672.71	1.10	−13.06	−55.16
744	35	42.47	120	29.53	1,199.0	979,678.63	.81	−14.36	−54.93
745	35	44.70	120	28.85	1,755.0	979,649.35	1.79	5.48	−53.27
746	35	43.40	120	28.31	1,541.0	979,658.80	1.03	−3.34	−55.48
747	35	45.60	120	22.99	2,113.0	979,629.27	1.80	17.78	−53.28
748	35	46.71	120	21.56	1,813.0	979,657.81	2.37	16.53	−43.64
749	35	45.89	120	20.97	1,681.0	979,664.63	1.24	12.10	−44.65
750	35	37.81	120	21.51	1,125.0	979,675.34	.40	−17.97	−56.40
751	35	36.44	120	20.68	1,130.0	979,670.81	.70	−20.08	−58.39
752	35	35.39	120	18.18	1,194.0	979,664.76	1.01	−18.62	−58.82
753	35	34.28	120	16.46	1,238.0	979,661.25	1.00	−16.41	−58.14

TABLE 2.—*Principal facts for gravity stations*—Continued

Station	Latitude N.		Longitude W.		Elevation (ft)	Observed gravity	Terrain correction	Free air anomaly	Complete Bouguer anomaly
	Deg	Min	Deg	Min					
754	35	33.39	120	15.22	1,269.0	979,658.12	0.86	−15.36	−58.30
755	35	36.86	120	18.90	1,271.0	979,661.19	1.26	−17.04	−59.64
756	35	37.99	120	15.49	1,826.0	979,647.51	1.39	19.87	−41.72
757	35	37.22	120	18.03	1,383,0	979,657.23	1.45	−10.98	−57.25
758	35	34.53	120	20.17	1,163.0	979,665.98	.79	−19.09	−58.44
759	35	33.20	120	19.94	1,208.0	979,661.94	.84	−17.01	−57.86
760	35	32.20	120	20.02	1,234.0	979,660.86	.92	−14.22	−55.89
761	35	30.31	120	19.94	1,284.0	979,660.26	.95	−7.43	−50.80
762	35	31.46	120	18.33	1,717.0	979,626.42	1.53	−2.19	−59.89
763	35	31.51	120	15.97	1,410.0	979,645.73	1.05	−11.82	−59.42
764	35	30.11	120	16.46	1,703.0	979,627.47	.81	−.53	−58.47
765	35	33.27	120	17.78	1,679.0	979,629.06	1.14	−5.69	−62.47
766	35	30.95	120	21.05	1,651.0	979,635.67	1.12	1.58	−54.26
767	35	32.94	120	22.00	1,595.0	979,638.38	1.07	−3.80	−57.76
768	35	34.24	120	22.21	1,470.0	979,647.90	1.16	−7.89	−57.45
769	35	35.64	120	21.86	1,385.0	979,654.16	.87	−11.61	−58.53
770	35	45.94	120	24.25	2,055.0	979,635.47	1.93	18.04	−50.89
771	35	48.79	120	25.50	2,316.0	979,625.16	2.76	28.22	−48.87
772	35	47.35	120	25.16	2,319.0	979,619.62	3.36	25.01	−51.58
773	35	48.36	120	27.21	2,304.0	979,622.39	3.16	24.93	−51.34
774	35	49.96	120	26.52	2,446.0	979,618.85	3.17	32.46	−48.69
775	35	51.37	120	25.29	1,644.0	979,679.23	1.42	15.41	−39.89
776	35	53.18	120	27.88	1,944.0	979,663.07	1.93	24.88	−40.24
777	35	52.53	120	28.95	2,508.0	979,622.75	2.66	38.53	−45.27
778	35	51.21	120	29.79	1,837.0	979,663.60	2.24	18.16	−42.96
780	35	49.20	120	29.11	2,035.0	979,639.84	1.71	15.89	−52.58
781	35	47.33	120	29.83	1,938.0	979,641.76	2.47	11.35	−53.02
815	35	32.36	120	13.76	1,264.0	979,657.16	.83	−15.33	−58.12
816	35	31.44	120	13.04	1,293.0	979,653.73	.85	−14.72	−58.50
817	35	30.33	120	13.63	1,440.0	979,642.27	.74	−10.78	−59.73
818	35	30.38	120	11.56	1,369.0	979,646.18	.97	−13.62	−59.89
819	35	30.18	120	9.36	1,704.0	979,623.52	.27	−4.49	−63.00
820	35	31.18	120	7.85	1,950,0	979,612.10	.48	5.80	−60.97
821	35	31.16	120	4.17	1,743.0	979,633.03	.92	7.30	−51.91
822	35	32.15	120	5.16	1,681.0	979,639.86	.62	6.89	−50.48
CRZOB	35	33.44	120	6.38	1,664.0	979,644.80	.48	8.40	−48.53
824	35	33.63	120	3.12	1,373.0	979,664.52	.67	.48	−46.23
825	35	34.24	120	1.08	1,218.0	979,669.65	.86	−9.84	−51.01
826	35	35.05	120	8.07	1,777.0	979,644.68	1.27	16.61	−43.41
827	35	36.36	120	9.48	1,924.0	979,638.77	1.27	22.67	−42.42
828	35	35.29	120	10.98	1,927.0	979,642.60	1.18	28.30	−36.98
829	35	39.03	120	10.64	2,196.0	979,632.63	1.48	38.31	−35.93
830	35	39.82	120	9.45	1,861.0	979,654.91	2.01	27.96	−34.22
831	35	40.75	120	8.59	1,185.0	979,697.23	1.99	5.38	−32.53
832	35	41.94	120	16.07	1,526.0	979,668.37	1.05	6.89	−44.71
833	35	40.74	120	14.77	1,788.6	979,652.24	1.15	17.17	−43.38
834	35	39.83	120	13.48	1,977.0	979,640.58	1.28	24.52	−42.38
835	35	38.18	120	12.12	1,957.0	979,641.46	.97	25.87	−40.65
836	35	38.62	120	13.63	2,213.0	979,623.57	1.48	31.43	−43.40
837	35	37.86	120	19.80	1,621.0	979,639.43	1.91	−7.30	−61.32
838	35	35.69	120	23.98	1,311.0	979,663.83	.69	−8.97	−53.52
839	35	34.59	120	23.78	1,398.0	979,656.09	.72	−6.97	−54.49
840	35	39.19	120	20.98	1,648.0	979,639.67	2.84	−6.42	−60.43
841	35	40.21	120	19.16	1,857.0	979,635.55	1.33	7.67	−55.06
842	35	40.82	120	17.26	2,128.0	979,625.58	2.54	22.31	−48.53
843	35	39.71	120	16.88	2,007.0	979,632.54	2.14	19.47	−47.60
844	35	36.89	120	14.36	2,288.0	979,612.81	1.62	30.18	−47.08
845	35	36.30	120	15.58	2,576.0	979,592.40	5.27	37.69	−45.83
846	35	34.68	120	14.78	2,107.0	979,613.84	3.45	17.33	−51.87
847	35	36.82	120	12.26	2,455.0	979,600.61	3.50	33.79	−47.34
848	35	35.18	120	12.57	2,068.0	979,623.25	2.15	22.37	−46.80
849	35	33.84	120	13.69	1,787.0	979,629.16	2.12	3.75	−55.77
850	35	33.27	120	12.09	2,058.0	979,609.62	2.56	10.51	−57.90
851	35	34.29	120	10.63	2,212.0	979,611.56	1.56	25.48	−49.23

TABLE 2.—*Principal facts for gravity stations*—Continued

Station	Latitude N.		Longitude W.		Elevation (ft)	Observed gravity	Terrain correction	Free air anomaly	Complete Bouguer anomaly
	Deg	Min	Deg	Min					
852	35	32.26	120	10.95	1,822.0	979,622.32	1.06	2.45	−59.33
853	35	32.28	120	8.98	2,027.0	979,611.11	1.33	10.49	−58.08
854	35	32.59	120	7.09	2,284.0	979,596.98	2.32	20.09	−56.34
855	35	30.24	120	6.43	2,327.0	979,583.92	1.47	14.41	−64.34
856	35	33.56	120	8.24	2,270.0	979,603.90	2.49	24.32	−51.46
857	35	43.25	120	16.47	1,225.0	979,693.50	.95	1.85	−39.48
858	35	44.65	120	18.36	1,550.0	979,668.71	2.21	5.63	−45.64
859	35	42.24	120	21.49	1,812.0	979,638.52	2.18	3.51	−56.81
860	35	43.59	120	21.93	1,895.0	979,638.41	1.68	9.29	−54.39
861	35	44.74	120	21.02	2,136.0	979,628.21	2.58	20.11	−50.96
862	35	43.57	120	19.49	1,913.0	979,641.40	2.20	14.00	−49.78
863	35	43.03	120	14.75	1,812.0	979,661.80	1.65	25.67	−35.18
864	35	43.03	120	13.33	2,052.0	979,644.62	1.68	31.06	−38.03
865	35	41.90	120	13.96	1,803.0	979,659.16	.94	23.79	−37.46
866	35	40.59	120	12.10	2,009.0	979,648.33	1.14	34.20	−33.94
867	35	41.16	120	10.62	2,512.0	979,610.64	5.40	43.00	−38.19
868	35	42.20	120	11.92	2,288.0	979,627.98	4.01	37.79	−37.08
869	35	44.76	120	11.58	1,703.0	979,673.50	1.75	24.65	−32.35
870	35	45.15	120	10.70	2,752.0	979,607.23	7.41	56.47	−30.96
871	35	44.65	120	9.35	2,713.0	979,609.54	7.55	55.83	−30.12
872	35	44.29	120	7.97	3,125.0	979,575.41	13.84	60.95	−32.86
873	35	44.36	120	6.60	1,886.0	979,660.22	2.90	29.15	−33.00
874	35	44.73	120	2.68	725.0	979,717.21	.35	−23.58	−48.26
875	35	43.93	120	4.45	1,009.0	979,707.11	.93	−5.83	−39.73
876	35	43.46	120	3.09	1,064.0	979,697.97	1.05	−9.12	−44.80
877	35	42.52	120	5.14	1,070.0	979,704.19	.90	−1.00	−37.03
878	35	41.75	120	.57	940.0	979,701.48	1.65	−14.84	−45.64
879	35	40.36	120	.56	642.0	979,719.86	.23	−22.51	−44.45
880	35	39.44	120	.03	659.0	979,711.85	.24	−27.61	−50.13
881	35	39.34	120	1.38	673.0	979,714.13	.36	−23.87	−46.75
882	35	40.37	120	2.68	726.0	979,718.36	.34	−16.12	−40.85
883	35	39.62	120	7.47	1,172.0	979,696.10	.95	4.63	−34.87
884	35	38.65	120	5.92	1,065.0	979,695.66	.90	−4.49	−40.35
885	35	37.99	120	4.23	1,263.0	979,680.16	.91	−.43	−43.11
886	35	37.39	120	1.92	1,387.0	979,661.89	2.61	−6.18	−51.43
887	35	36.87	120	.56	893.0	979,692.15	.63	−21.65	−51.85
888	35	35.71	120	2.49	1,140.0	979,674.04	1.02	−14.87	−53.20
889	35	36.86	120	2.98	1,071.0	979,689.24	.81	−7.80	−43.96
890	35	36.31	120	5.26	2,031.0	979,626.85	2.09	20.88	−47.07
891	35	36.34	120	7.12	2,021.0	979,630.84	1.35	23.89	−44.46
892	35	37.83	120	6.74	1,754.0	979,646.32	3.27	12.14	−45.10
893	35	37.67	120	8.27	2,137.0	979,627.26	2.82	29.32	−41.55
894	35	34.70	120	3.54	2,014.0	979,620.45	3.47	15.17	−50.82
895	35	35.06	120	5.97	2,036.0	979,625.23	1.69	21.51	−47.02
896	35	30.78	120	.93	2,621.0	979,579.10	2.94	36.47	−50.92
897	35	32.50	120	3.20	2,106.0	979,615.40	2.75	21.90	−47.97
898	35	32.45	120	.58	2,245.0	979,600.11	5.21	19.75	−52.44
913	35	54.77	120	28.22	1,779.0	979,670.96	1.36	14.98	−45.02
914	35	54.09	120	29.77	2,145.0	979,652.17	2.51	31.58	−39.87
916	35	56.91	120	28.39	1,757.0	979,666.08	1.88	4.98	−53.75
917	35	58.47	120	29.48	2,088.0	979,647.81	2.85	15.61	−53.54
918	35	56.22	120	25.59	1,661.0	979,675.38	2.78	6.24	−48.28
919	35	57.76	120	25.77	3,467.0	979,560.04	11.18	58.52	−49.70
920	35	46.77	120	14.06	1,921.0	979,664.45	2.07	33.24	−30.94
921	35	47.33	120	6.69	849.0	979,724.38	.89	−8.45	−36.87
922	35	49.06	120	6.52	847.0	979,714.37	.66	−21.11	−49.70
923	35	50.92	120	6.85	784.0	979,711.57	.49	−32.49	−59.07
924	35	52.09	120	9.48	1,110.0	979,700.48	1.52	−14.59	−51.38
925	35	52.30	120	11.80	1,149.0	979,706.72	2.89	−4.98	−41.75
926	35	50.59	120	5.04	746.0	979,709.45	.29	−37.72	−63.18
927	35	49.95	120	3.43	686.0	979,712.25	.17	−39.65	−63.16
928	35	52.16	120	2.03	535.0	979,717.55	.09	−51.70	−70.09
929	35	50.84	120	1.24	527.0	979,717.23	.07	−50.89	−69.02

TABLE 2.—*Principal facts for gravity stations*—Continued

Station	Latitude N.		Longitude W.		Elevation (ft)	Observed gravity	Terrain correction	Free air anomaly	Complete Bouguer anomaly
	Deg	Min	Deg	Min					
930	35	49.10	120	0.21	528.0	979,714.91	0.06	−50.64	−68.81
931	35	48.92	120	1.69	932.0	979,691.89	.93	−35.40	−66.64
932	35	47.74	120	.94	869.0	979,695.69	2.51	−35.84	−63.33
933	35	46.45	120	2.69	612.0	979,716.14	.22	−37.73	−58.64
934	35	45.87	120	4.69	806.0	979,719.41	.68	−15.38	−42.53
AVNLB	35	59.54	120	7.65	754.0	979,714.36	.27	−44.83	−70.59
936	35	59.58	120	9.82	824.0	979,711.87	.41	−40.79	−68.83
937	35	59.57	120	11.93	931.0	979,710.06	.72	−32.53	−63.95
938	35	59.70	120	14.83	1,301.0	979,694.69	1.47	−13.28	−56.71
939	35	58.07	120	15.23	1,554.0	979,684.73	3.76	2.88	−46.97
940	35	59.17	120	16.83	1,735.0	979,674.28	2.93	7.88	−49.04
941	35	57.81	120	9.80	1,017.0	979,701.54	.74	−30.44	−64.81
942	35	54.92	120	11.29	1,915.0	979,659.58	1.93	16.18	−47.94
943	35	54.25	120	13.72	1,429.0	979,691.69	3.48	3.54	−42.29
944	35	54.48	120	8.92	1,280.0	979,693.01	1.11	−9.48	−52.55
945	35	56.43	120	10.68	1,756.0	979,661.93	3.23	1.42	−55.92
946	35	57.87	120	7.69	813.0	979,710.70	.50	−40.56	−68.13
964	35	55.09	120	24.27	2,249.0	979,638.61	2.61	26.38	−48.56
965	35	53.79	120	23.88	1,683.0	979,677.78	1.48	14.18	−42.40
966	35	52.71	120	22.73	1,531.0	979,690.52	1.25	14.16	−37.41
967	35	52.47	120	19.76	1,637.0	979,684.75	1.74	18.70	−36.03
968	35	51.38	120	16.62	1,657.0	979,687.97	1.44	25.36	−30.37
969	35	50.22	120	17.76	1,489.0	979,700.87	.93	24.11	−26.33
970	35	48.53	120	16.96	1,515.0	979,701.27	.89	29.37	−22.01
971	35	47.27	120	17.62	1,313.0	979,713.65	.89	24.55	−19.87
972	35	45.38	120	15.85	1,375.0	979,696.47	.85	15.89	−30.71
973	35	46.42	120	10.46	1,482.0	979,692.16	1.93	20.16	−29.04
974	35	47.10	120	10.88	1,575.0	979,685.62	1.49	21.40	−31.45
975	35	48.91	120	12.13	1,741.0	979,677.39	1.44	26.20	−32.42
976	35	50.29	120	12.00	1,441.0	979,692.24	2.54	10.87	−36.31
977	35	51.21	120	12.11	1,260.0	979,702.13	3.51	2.42	−37.55
978	35	51.96	120	14.14	3,052.0	979,586.35	10.08	54.09	−40.98
979	35	48.12	120	13.03	2,535.0	979,629.60	5.03	54.21	−28.14
980	35	49.40	120	13.81	2,290.0	979,647.12	2.31	46.86	−29.78
981	35	50.05	120	15.02	2,440.0	979,637.60	3.88	50.52	−29.71
982	35	53.38	120	2.77	559.0	979,719.47	.16	−49.27	−68.41
D-1	35	45.84	120	18.16	1,141.0	979,701.84	.70	−1.40	−40.08
D-2	35	46.08	120	18.07	1,142.0	979,703.72	.68	.23	−38.51
D-3	35	46.33	120	17.98	1,146.0	979,707.32	.68	3.85	−35.02
D-4	35	46.59	120	17.88	1,154.0	979,711.44	.72	8.35	−30.76
D-5	35	46.97	120	17.73	1,196.0	979,717.65	.79	17.97	−22.52
D-6	35	46.76	120	17.81	1,170.0	979,717.29	.73	15.46	−24.19
983	35	46.91	120	18.15	1,171.0	979,716.91	.79	14.97	−24.66
984	35	45.98	120	16.84	1,186.0	979,710.72	.76	11.51	−28.66
985	35	47.56	120	15.73	1,792.0	979,679.01	2.48	34.54	−24.79
986	35	49.22	120	18.68	1,715.0	979,687.18	1.79	33.10	−24.27
987	35	49.85	120	20.95	1,660.0	979,695.98	3.54	35.83	−17.89
988	35	54.57	120	20.20	3,007.0	979,593.17	4.72	52.96	−45.93
989	35	54.39	120	18.86	3,177.0	979,580.42	5.79	56.45	−47.21
990	35	55.26	120	21.65	3,172.0	979,581.11	4.84	55.43	−49.01
991	35	57.65	120	27.06	2,705.0	979,605.76	5.29	32.75	−55.18
992	35	56.34	120	20.36	4,339.0	979,500.51	17.33	83.00	−48.97
993	35	58.50	120	24.98	3,426.0	979,568.88	7.33	62.45	−48.21
994	35	58.07	120	23.56	3,764.0	979,539.31	15.16	65.27	−49.16
995	35	48.01	120	9.21	2,658.0	979,608.19	13.75	44.52	−33.34
996	35	50.38	120	10.75	2,640.0	979,608.66	10.85	39.92	−40.22
997	35	53.06	120	6.87	976.0	979,702.32	.47	−26.74	−59.96
998	35	52.64	120	4.49	762.0	979,711.66	.26	−36.93	−62.98
999	35	54.39	120	5.55	913.0	979,700.84	.56	−36.04	−67.00
1000	35	55.75	120	6.68	872.0	979,706.71	.51	−35.97	−65.56
1001	35	52.63	120	.18	466.0	979,720.96	.04	−55.45	−71.51
1002	35	54.25	120	.42	701.0	979,708.18	.33	−48.44	−72.32
1003	35	54.86	120	1.81	521.0	979,719.90	.05	−54.52	−72.47
1004	35	55.29	120	14.53	1,642.0	979,679.18	3.85	9.58	−43.22
1005	35	55.76	120	15.25	1,740.0	979,673.34	4.53	12.28	−43.21

TABLE 2.—*Principal facts for gravity stations*—Continued

Station	Latitude N.		Longitude W.		Elevation (ft)	Observed gravity	Terrain correction	Free air anomaly	Complete Bouguer anomaly
	Deg	Min	Deg	Min					
1006	35	57.10	120	15.81	2,670.0	979,618.44	4.56	42.93	−44.54
1007	35	56.82	120	14.82	3,078.0	979,583.48	12.01	46.73	−47.30
1008	35	57.15	120	16.67	2,951.0	979,600.56	5.46	51.40	−44.82
1009	35	57.63	120	17.89	2,719.0	979,616.79	4.33	45.13	−44.25
1010	35	54.36	120	16.50	3,473.0	979,559.53	8.59	63.43	−47.58
1011	35	53.03	120	14.86	2,811.0	979,606.12	5.27	49.67	−41.92
1014	35	59.95	120	19.07	1,334.0	979,702.33	4.19	−2.90	−44.74
1015	35	58.94	120	19.17	1,667.0	979,682.32	6.68	9.86	−40.97
1016	35	58.22	120	19.39	1,937.0	979,665.28	6.10	19.24	−41.47
1017	35	56.99	120	5.55	710.0	979,712.43	.25	−47.26	−71.52
1018	35	56.11	120	3.39	576.0	979,717.39	.09	−53.64	−73.45
1019	35	56.41	120	.69	744.0	979,711.23	.37	−44.43	−69.75
1020	35	57.46	120	.37	754.0	979,715.14	.26	−41.08	−66.85
1021	35	58.68	120	1.25	1,054.0	979,697.74	.80	−32.01	−67.59
1022	35	59.57	120	.18	767.0	979,717.42	.42	−40.59	−66.65
1023	35	59.76	120	2.14	1,062.0	979,698.15	.98	−32.39	−68.06
1025	35	59.87	120	4.64	1,109.0	979,692.68	1.38	−33.59	−70.49
1026	35	57.85	120	4.43	671.0	979,715.12	.17	−49.46	−72.46
1027	35	59.60	120	6.08	790.0	979,713.19	.26	−42.70	−69.72

station) terrain corrections were made manually by using Hayford-Bowie templates. (See Swick, 1942.) Where corrections were unusually large, individual compartments of these templates were divided into subcompartments according to a scheme developed by H. W. Oliver of the Geological Survey. For the outer zones the corrections were made by a digital computer program developed by Plouff (1966), which employed 1- and 3-minute terrain digitization grids on topographic maps.

Observed gravity values were converted to anomaly values using a gravity-reduction program developed by S. H. Burch. The basic procedures and formulas of the reduction are as follows, where gravity values are in milligals:

1. The gravity difference ($\triangle G$) between the base and a given station is calculated and corrected for lunar and solar tide and instrument drift.
2. Observed gravity (OG) equals gravity base value + $\triangle G$.
3. Theoretical gravity (THG) equals $978{,}049\ [1+0.005228\ \sin^2\theta-0.0000059\ \sin^2(2\theta)]$, where θ equals latitude in degrees.
4. Free air anomaly (FAA) equals $OG-THG+(0.09411549-0.000137789\ \sin^2\theta)\mathrm{E}-0.0000000067E^2$, where E equals elevation in feet above sea level.
5. Simple Bouguer anomaly (BA) equals $FAA-0.012774\rho E$, where ρ equals reduction density, in grams per cubic centimeter.
6. Curvature correction (CC) equals $0.000446E-3.28\times10^{-8}E^2+1.27\times10^{-15}E^3$.
7. Complete Bouguer anomaly (CBA) equals $BA+TC-CC$, where TC equals terrain correction.

GRAVITY INTERPRETATION

Quantitative interpretation of gravity data here is based largely on two-dimensional crustal models constructed with the use of computer programs of Bott (1960) and Talwani. (See Talwani and others, 1959.) Corrections for finite strike length of these models were made using graticule methods of Henderson and Zietz (1957) and a computer program of Talwani and Ewing (1960) for three-dimensional bodies. Preliminary calculations of anomalous subsurface mass were made by using a program based on the two-dimensional program of Bott (1960).

Density contrasts used to analyze anomalous gravity features are average or median values based in part on data of Bailey and others (1964), Burch (1965), Byerly (1966), Clement (1965), and D. C. Ross (oral commun., 1969). Estimates of average densities used for various lithologic units conform generally to those used in nearby areas (Burch and Durham, 1970; Burch, 1971; Burch and others, 1971), and the following ranges of values, except where they apply to "surficial deposits," may be interpreted as wet bulk densities:

Lithologic unit	*Average density (g/cm³)*
Surficial deposits	1.4–2.0
Paso Robles and Tulare Formations	2.2
Upper Miocene and Pliocene rocks	2.2–2.3
Monterey Shale	2.3
Lower and middle Miocene rocks	2.4
Eocene and Upper Cretaceous rocks	2.5–2.6
Serpentinized ultramafic rocks	≈2.5
Franciscan rocks	2.6–2.8
Granitic rocks	2.6–2.9

In first approximations of subsurface mass distributions, a density contrast of 0.5 g/cm^3 was assumed between either Franciscan or Salinian basement rocks and overlying post-Eocene rocks, and a density contrast of 0.3 g/cm^3 was assumed between either Franciscan or Salinian basement rocks and overlying pre-Eocene rocks. Effective models for subsurface distributions of mass were ultimately based on "lumped" average densities for Quaternary sedimentary rocks and deposits and for most Tertiary sedimentary rocks. The lithologic breakdown of densities used in this report conforms to similar density units used in gravity studies to the west. (See Burch, 1971; Burch and Durham, 1970.)

MAGNETIC SURVEYS

Aeromagnetic data within the map area are part of a reconnaissance survey of part of the San Andreas fault. (See Hanna, 1968a.) The flight pattern of the reconnaissance survey consists of seven traverses 4 miles apart parallel to the San Andreas fault between San Francisco and San Benardino. The central flight line follows the surface trace of the fault. A single transverse line was flown about 5 miles southeast of Parkfield within the map area. The total intensity contoured data (pl. 2) consist of digitally recorded output from an ASQ–10 fluxgate magnetometer flown at 6,500 feet barometric elevation. Flight paths were recovered using an APN–147 Doppler system and were checked with a strip-film camera. A regional magnetic field of 9 gammas per mile in the direction N. 16° E. was removed from the aeromagnetic map.

Vertical-intensity ground magnetic data were collected over the southern two-thirds of the map area and are presented as a 50-gamma contour map. (See pl. 3.) Measurements were made with a Sharpe model MF–1R–100 fluxgate magnetometer having a maximum sensitivity of about ±2 gammas. Approximately 150 stations were read and tied to six secondary base stations that were adjusted relative to a primary base station near Shandon. Multiple readings of stations within the network indicate a precision of about ±15 gammas for most of the survey. The azimuth of the instrument was kept at a fixed angle relative to magnetic north in order to avoid "heading" errors. Local magnetic fields generated by an extensive network of pipelines and a number of well casings south of Cholame were carefully avoided during the ground magnetic work. A regional magnetic field of 15 gammas per mile in the direction N. 16° E. was removed from the map.

MAGNETIC INTERPRETATION

Magnetic data were analyzed with the assistance of digital computer programs for calculating total- and vertical-intensity magnetic fields over two- and three-dimensional bodies. Regional magnetic gradients of the vertical and total fields, due primarily to the dipolar nature of the field produced by the earth's core, were subtracted from the observed data using U.S. Coast and Geodetic Survey magnetic charts. An induction-type apparatus (Hanna, 1968b) was used to measure magnetic susceptibilities of selected rock specimens.

Magnetization contrasts used in analyzing anomalous magnetic features are estimated average values partly based on data of Burch (1965), Saad (1968), and DuBois (1963) and partly based on data presented in this report. In the present study, total magnetization (induced plus remanent) contrasts of 0.0005 to 0.0050 emu/cm^3 (electromagnetic units per cubic centimeter) were assumed between serpentinites and surrounding rocks. Although Salinian basement rocks may have magnetizations of as much as 0.001 to 0.005 emu/cm^3 locally within the map area, a probable average magnetization value for most of these rocks is 0.0001 emu/cm^3 or less, considerably lower than values for magnetic rocks near Table Mountain and Palo Prieto Pass.

GEOLOGIC SETTING

The mapped area is separated into two major tectonic units by the northwest-trending San Andreas fault (pl. 1), probably California's most spectacular and widely known structural feature. Tens and perhaps hundreds, of miles of right-lateral strike-slip movement have taken place on the San Andreas in Cenozoic time (Hill and Dibblee, 1953; Crowell, 1962; Dickinson and Grantz, 1968), and it has been the source of major and recurring earthquakes in recent historic time. Within the mapped area, active right-lateral strike slip on the San Andreas fault is indicated by (1) prominent offset of stream channels and other features, (2) measurable offset of triangulation networks (Burford, 1966; Howard, 1968), and (3) offset of manmade features and surface ruptures formed during the 1966 Parkfield-Cholame earthquake. (See Brown and others, 1967.)

The tectonic unit northeast of the San Andreas fault includes the southeastern Diablo Range and northwestern Temblor Range. Pervasively sheared rocks of Mesozoic age composed of Franciscan rocks and associated ultramafic rocks constitute the "basement" of this terrane. Owing to its pervasively sheared condition, this "basement" is plastic and is

structurally overlain by approximately 18,000 feet of marine sedimentary rocks of Tertiary and Cretaceous age, which in turn is overlain by nearly 3,000 feet of Quaternary valley sediments.

The region southwest of the San Andreas fault is an area of low hills that are transected by and drain into Cholame and San Juan Creeks, which empty into the Salinas River. It is part of the "Salinia" block of Reed (1933, p. 21) or Salinian block of Compton (1966), of which the basement is composed of crystalline rocks made up of plutonic rocks of Mesozoic age and local pendants of older metasedimentary rocks. Because of its crystalline texture, this basement is moderately rigid. It is overlain by roughly 4,500 feet of Tertiary sedimentary rocks, which in turn are unconformably overlain by Quaternary valley sediments as thick as 3,000 feet.

Rock units are lumped to conform with similar units of the generalized geologic maps used for gravity interpretation to the west. (See Burch and Durham, 1970; Burch, 1971.) The main purpose of combining rock units in this fashion is to facilitate geophysical interpretation. Because the lumping of units was in places arbitrary and because these units appear on similar generalized geologic maps to the west, it is necessary to describe in some detail the lithologic and structural features of the units as they occur within the map area.

ROCK UNITS

PLUTONIC AND METAMORPHIC ROCKS

Within the mapped area the basement of the Salinian block is composed mainly of plutonic rocks and a few small lenses, pendants, and xenoliths of gneiss, schist, and marble. These basement rocks crop out in the Red Hills and at several places near Parkfield; they were penetrated by 11 exploratory wells (Nos. 1, 11, 18, 19, 20, 31, 39, 40, 42, 44, and 47 on pl. 1 and in table 3). The most prominent exposures are in the Red Hills, where the rock is a gray, medium-grained, somewhat gneissoid quartz diorite containing roughly 15 percent biotite and lesser amounts of hornblende. Outcrops of granodiorite with less biotite occur about 4 miles west of Parkfield. The granitic rock penetrated in the six exploratory wells ranges from granodiorite to hornblende-rich diorite. Granodiorite is exposed extensively in the LaPanza Range southwest of the map area.

In addition to their occurrence west of the San Andreas fault, plutonic rocks are found in the fault block between the San Andreas and Gold Hill faults. The small exposures near Middle Mountain northwest of Parkfield are composed of granitic rocks and pendants of marble and schist that are typical of basement rocks west of the San Andreas fault. However, the outcrops at Gold Hill differ in that they are mainly hornblende quartz gabbro composed of hornblende and calcic plagioclase in nearly equal amounts, a small percentage of quartz (Ross, 1970), and a very small mass of marble. The age of the gabbro was estimated by the potassium-argon method to be about 143 million years. (See Hay, 1963, p. 113–115.) This age is similar to ages obtained for plutonic rocks of the foothills of the Sierra Nevada, yet it differs greatly from the age of 80.5 million years obtained for areas of basement rocks in the LaPanza Range to the west. (See Hay, 1963, p. 113.)

Densities of plutonic rocks of the Salinian block are assumed to average 2.6 to 2.7 g/cm^3; those of associated metamorphic rocks may be as much as 3.2 g/cm^3 if the rocks are comparable to schists from the Salinian block outside of the map area. (See Compton, 1964, p. 281.) The hornblende quartz gabbro of Gold Hill averages 2.90 g/cm^3, based on densities for nine samples of D. C. Ross (oral commun., 1969).

The magnetizations of Salinian plutonic rocks in the map area probably average about 0.0005 emu/cm^3 or less. Metamorphic rocks are generally nonmagnetic relative to the plutonic rocks. Measured susceptibilities of hornblende quartz gabbro from a single outcrop at Gold Hill average 0.0001 emu/cm^3 or less, although the value of one sample exceeds 0.0010 emu/cm^3.

ULTRAMAFIC ROCKS

The ultramafic rocks are commonly emplaced along faults and within Franciscan rocks. Most are serpentinites typical of those found throughout Franciscan terrane. (See Bailey and Everhart, 1964, p. 47.) The smaller bodies are thoroughly serpentinized, and intense shearing has destroyed original textures in all but a few small remnant blocks. The centers of the larger bodies consist of blocky serpentinite, but invariably this material grades outward to the usual sheared serpentinite. These serpentinite bodies crop out as elongate pods, lenses, or sheets generally concordant with the regional structure. They commonly form discontinuous trains that extend many miles, probably along major fault zones. In a few places the serpentinite contains small masses of medium- to coarse-grained diabase composed mainly of hornblende and plagio-

TABLE 3.—*Selected exploratory wells*

[Compilation by H. C. Wagner. Elevation measured from the following: KB, Kelly bushing; GR, ground; DF, derrick floor. T, data obtained from topographic map]

No. on pl. 1	Operator	Well	Location			Year drilled	Elevation (feet)	Total depth (feet)	Reported geologic data (depths in feet)
			Section	Township south	Range east				
1	Cholame Valley Oil and Development Co.	1	31	22	14	Pre-1900	2,000 T	950	Bottom in granite.
2	Occidental Petroleum Corp	Kreyenhagen 24	28	22	16	1963	1,214 KB	6,350	Bottom in Eocene. Top of Eocene, 55.
3	Kettleman North Dome Association	76	34	22	18	1931	807 GR	9,206	Bottom in lower Miocene.
4	Slayton Drilling Co	Colgrove-Taylor 88-15	15	23	14	1948	1,600 T	4,996	Bottom in Cretaceous.
5	Future Success Co	Livermore 1	18	23	15	--	2,600 T	1,815	Bottom in Franciscan serpentine.
6	Canadian Co	1	19	23	15	--	2,700 T	250	Do.
7	Pacific Inland Oil Co	1	19	23	15	1936	2,300 T	3,100	Do.
8	Shell Oil Co	Crow 41-2	2	23	16	1944	1,189 DF	7,825	Bottom in Eocene or Cretaceous.
9	Sunray DX Oil Co.	Lynch-Mouren 68-9	9	23	17	1950	1,089 KB	11,962	Bottom in lower Miocene.
10	Knudsen-Schmidt Co	Avenal 1	36	23	17	1932	800 T	6,854	Bottom in Eocene.
11	A. A. Anderson	Hillman 1	15	24	14	1938	2,400 T	4,006	Bottom in granite. Top of granite, 3,970.
12	Humble Oil & Refining Co	Avenal Land & Oil Co. 5	3	24	17	1961	861 KB	5,338	Bottom in upper Cretaceous (Panoche).
13	do	Orchard 3-1	12	24	17	1959	789 KB	5,866	Do.
14	Ancora Corp	Capital 2	16	23	18	1953	673 DF(?)	6,148	Bottom in Oligocene.
15	Amerada Petroleum Corp	Malley 1	22	23	18	1958	660 T	6,301	Bottom in upper Miocene.
16	Bell Petroleum Co	Orchard 37-30	30	23	18	1958	690 KB	6,461	Bottom in upper Cretaceous.
17	Havenstrite Oil Co	Havenstrite-Cleary 1	8	25	14	1953	1,690 KB	6,236	Bottom in Oligocene red beds.
18	Socony-Mobil	Hillman-Darnall 22-34	34	25	14	1951	1,385 KB	7,716	Bottom in granite. Top of granite, 7,660.
19	Cholame Syndicate	Jack 2	10	25	15	1934	1,650 T	3,867	Bottom in granite. Top of granite, 3,650.
20	Continental Oil Co	Taylor 1	23	25	15	1949	1,720 T	6,559	Bottom in granite. Top of grante, 6,523.
21	C. W. Colgrove	Jack 18-3	3	25	16	1949	1,570 KB	2,737	Bottom in Cretaceous. Top of Cretaceous, 2,010.
22	Franco Western	Jack 1	8	25	16	1949	1,185 KB	1,490	Bottom in Franciscan. Top of Franciscan, 1,297.
23	C. W. Colgrove	Jack 17-16	16	25	16	1950	1,360 T	1,850	Bottom in Franciscan. Top of Franciscan, 1,370.
24	do	Jack 83-17	17	25	16	1950	1,384 KB	2,810	Bottom in Franciscan. Top of Franciscan, 2,802.
25	Keloil, Inc	Keller 1	17	25	16	1949	1,180 GR	2,025	Bottom in schist. Top of schist, 1,987.
26	Buass Development Co	Jack 1	19	25	16	1946	1,146 DF	3,405	Bottom in Franciscan. Top of Franciscan, 980.
27	C. W. Colgrove	Jack 32-21	21	25	16	1954	1,400 T	4,997	Bottom in Franciscan. Top of Franciscan, 4,997.
28	D. C. Basdo, Jr	Jack 1-2	2	25	17	1959	859 KB	3,156	Bottom in Cretaceous. Top of Cretaceous, 200±.
29	C. H. Bent	D. B. 1	7	25	18	1954	675 T	2,516	Bottom in Cretaceous. Top of Cretaceous, 2,440.
30	Tidewater Oil Co	Levis 1	15	25	18	1952	619 KB	4,423	Bottom in Cretaceous. Top of Cretaceous, 4,278.
31	General Petroleum Corp	Clarke 84-25	25	26	14	1950	1,127 KB	5,687	Bottom in granite. Top of granite, 5,657.
32	Humble Oil & Refining Co	Hillman 1	32	26	14	1957	1,400 T	5,068	Bottom in lower Miocene.
33	Tutin and Twisselman	White 1	5	26	15	1945	1,300 T	5,509	Bottom in upper Miocene.
34	Amerada Petroleum Corp	Still B-1	3	26	17	1950	1,084 KB	4,199	Bottom in Cretaceous.
35	W. H. Davis	1	13	26	17	1927	900 T	3,250	Bottom in Cretaceous. Top of Cretaceous, 1,350.
36	Garner-Jones Operator	Still 1	30	26	17	1962	2,280 T	1,815	Bottom in Franciscan. Top of schist, 1,630.
37	Richard O. Maze	K. O. 1	3	26	18	1958	708 KB	4,636	Bottom in Cretaceous. Top of Cretaceous, 2,850.
38	Humble Oil & Refining Co	Newsom 1	20	26	18	1961	837 KB	5,082	Do.
39	do	Clarke 1	10	27	14	1958	1,465 KB	4,505	Bottom in granite. Top of granite, 4,320.
40	Texas Co	Clarke NCT-1 1	15	27	14	1955	1,435 KB	4,333	Bottom in granite. Top of granite, 4,078.
41	do	O'Donovan 1	21	27	14	1949	1,512 KB	2,803	Bottom in Oligocene(?). Top of red beds, 2,470.
42	Vanguard Oil Co	Clarke 1	26	27	14	1937	1,685 T	5,000	Bottom in granite. Top of granite, 4,949.
43	Latin American Oil Co	Upton 1	31	27	15	1925(?)	1,325 T	4,618	Bottom in lower Miocene. Top of lower Miocene, 4,335.
44	Texas Co	Iverson 1	15	27	16	1956	1,738 KB	2,426	Bottom in granite. Top of granite, 2,416.
45	Brookline Oil Co	McCornack-Vicki 1	16	27	16	1956	1,511 KB	6,016	Bottom in Oligocene(?). Top of red beds, 5,026.
46	Texas Co	Cammatta Ranch 2	29	27	16	1955	1,316 KB	6,015	Bottom in lower Miocene.
47	Shell Oil Co	Grant Estate C.H. 87-17	17	27	17	1949	2,030 T	2,993	Bottom in granite, Top of granite, 2,608.
48	T. V. Bergman	Bergman 1	5	27	18	1949	1,392 KB	7,141	Bottom in Cretaceous. Top of Cretaceous, 7,129.
49	Sunset Internat. Petroleum Corp	Shell USL 1	17	27	18	1957	1,709 KB	2,897	Bottom in Cretaceous. Top of Cretaceous, 1,610.

clase. The largest of these is in a quarry one-half of a mile west of the Antelope pumping station near Polonio Pass.

Densities of serpentinized ultramafic rocks vary considerably within the mapped area, the lowest values occurring in highly sheared rocks at Table Mountain. For purposes of gravity interpretation, a wet bulk density range of 2.3 to 2.5 g/cm^3 was assumed for anomaly-producing serpentinites within the mapped area.

Measured magnetic susceptibility values of serpentinized rocks within the mapped area fall into two distinct groups: one of about 1 to 4×10^{-3} emu/cm^3 and another of about 5×10^{-4} emu/cm^3. The most highly sheared, mechanically incompetent serpentinites of Table Mountain possess the strongest

induced magnetizations. Remanent magnetization was not measured, mainly because of the difficulty of finding material sufficiently coherent for collection and subsequent drilling. For interpretation purposes, serpentinites were assumed to have a total magnetization intensity range of 0.002 to 0.005 emu/cm ^{3}. Because magnetic intensities of ultramafic rocks increase with degree of serpentinization (Burch, 1965; Saad, 1968), the average magnetizations of serpentinite bodies may be strongly a function of depth below ground surface or distance from the center of the body.

FRANCISCAN ROCKS

Eugeosynclinal Franciscan rocks lie structurally below younger Cretaceous rocks in the Diablo and Temblor Ranges. In this area Franciscan rocks consist of a pervasively sheared assemblage of eugeosynclinal sedimentary and mafic volcanic rocks. They are composed of large and small shattered lenticular masses or monoliths of graywacke, greenstone, chert, and a few small blocks of glaucophane schist in a matrix of pervasively sheared argillaceous shale or claystone. The lenticular masses are generally oriented parallel to the shear planes of the matrix, which generally strike northwest and dip northeast, mainly at high angles. In the mapped area Franciscan rocks were described by Dickinson (1966a, p. 462) as an intensively deformed "tectonic breccia."

Owing to the pervasively sheared condition of the breccia, the thickness of Franciscan rocks here is difficult to estimate. Its age is not definitely known but is presumed to be Late Jurassic to Late Cretaceous on the basic of fossils reported from Franciscan rocks elsewhere. (See Bailey and others, 1964, fig. 23.)

Densities of various Franciscan lithologies are estimated to range from about 2.0 to 3.2 g/cm ^{3}. Measurements of Bailey, Irwin, and Jones (1964, pl. 2) on 16 graywacke samples clustered 9 miles north-northwest and 7 miles east of Parkfield (10 samples are within the mapped area, 7 are just north of the area) give an average density of 2.65 g/cm ^{3}, excluding an anomalously low value of 2.34 g/cm ^{3} for a single sample north of the map area. Greenstones are assumed to average about 2.8 g/cm ^{3} on the basis of Clement's data (1965); chert, about 2.65 g/cm ^{3}, the average density of quartz. Small blocks of glaucophane schist have densities that may average 3.0 to 3.2 g/cm ^{3} on the basis of data of Borg (1956) and Bloxam (1959, 1960). Argillaceous shale and claystone are assumed to have densities that range from about 2.0 to 2.5 g/cm ^{3}.

It is clear that no single density can adequately characterize the Franciscan rock assemblage in the mapped area. For purposes of gravity interpretation, however, an average density of 2.65 to 2.70 g/cm ^{3} was found to be reasonable over much of the area.

Except for local occurrences of greenstone that have average total magnetizations probably less than 0.0005 emu/em ^{3}, Franciscan rocks are believed to be relatively nonmagnetic in the mapped area.

CRETACEOUS AND EOCENE MIOGEOSYNCLINAL ROCKS

Northeast of the San Andreas fault pervasively sheared Franciscan rocks and ultramafic rocks are overlain, either unconformably or tectonically, by a thick series of miogeosynclinal marine clastic sedimentary rocks of Cretaceous and Eocene age. This series as defined by Dibblee (1972) was divided into two major sequences, one of Cretaceous age and one of early Tertiary (Eocene) age. Because these sequences are of about the same density, they are grouped on the map as one unit (pl. 1).

The lower sequence, defined by Dibblee (1972) as the Cretaceous marine sedimentary sequence and also known as the "Great Valley sequence" (Bailey and others, 1964, p. 123), consists of as much as 10,500 feet of strata. It is composed of two distinct units, in ascending order: (1) Badger Shale of Marsh (1960), dark argillaceous shale and thin interbeds of graywacke, as thick as 3,900 feet, of Early Cretaceous (?) age, and (2) Panoche Formation, interbedded argillaceous shale and sandstone, as thick as 6,800 feet, of Late Cretaceous age.

The upper sequence, defined as the lower Tertiary marine sedimentary sequence, unconformably overlies the Cretaceous sequence, is mainly of Eocene age, and is composed of two units, in ascending order: (1) Avenal Sandstone, including Acebedo Sandstone of Dickinson (1966a), about 300 feet thick, middle Eocene, and (2) Kreyenhagen Shale and Point of Rocks Sandstone (probably stratigraphic equivalents or facies) totaling about 3,000 feet thick, middle and upper Eocene, and in part Oligocene.

In the strip between the San Andreas and Gold Hill faults, about 2,000 feet of massive marine sandstone of probable Eocene age overlies hornblende quartz gabbro.

Densities of the Cretaceous and Eocene shales and sandstones probably range from about 2.1 to 2.7 g/cm ^{3} on the basis of data of Byerly (1966) for

an area to the north. In the present investigation, an average density range of 2.5 to 2.65 g/cm^3 was assumed for these rocks.

Magnetizations of the Cretaceous and Eocene sedimentary rocks are negligibly small.

MIDDLE AND UPPER TERTIARY ROCKS

DISTRIBUTION

Sedimentary rocks of middle and late Tertiary age occur extensively on both sides of the San Andreas fault and are composed of two sedimentary sequences as defined by Dibblee (1972). The lower one, of Oligocene and Miocene age, is composed of clastic sedimentary rocks and a low-density unit of siliceous shale. The upper unit, mainly of Pliocene age, is composed of clastic sedimentary rocks. In this report this series of middle and upper Tertiary sedimentary rocks is divided into two units of clastic sedimentary rocks separated by the siliceous shale unit. These units are, in ascending order: lower Miocene deposits, Monterey Shale, and upper Miocene and Pliocene deposits. In addition to these sedimentary rocks, there is a local volcanic unit of Miocene age which is not shown on the map.

Densities of middle and upper Tertiary rocks fall within the range 1.4 to 2.6 g/cm^3, although average density values used in gravity interpretation are restricted to the range 2.2 to 2.4 g/cm^3.

All middle and upper Tertiary rocks in the mapped area, including volcanic rocks, may be considered nonmagnetic for purposes of interpretation.

VOLCANIC ROCKS

Silicic volcanic rocks, radiometrically dated by Turner (1970) as being about 23.5 million years old, or of Oligocene age, crop out west of the San Andreas fault near Parkfield. These rocks are composed of perlitic obsidian and rhyolite that are probably of both intrusive and extrusive origin. They are intruded through, and extruded onto, granitic basement and are unconformably overlain by Santa Margarita Formation. A small dike of basalt crops out east of the fault near Franciscan Creek at the northern edge of Miller flats, south of Barrel Valley.

LOWER MIOCENE SEDIMENTARY ROCKS

Clastic sedimentary rocks of early Miocene age are present on both sides of the San Andreas fault. Northeast of the fault they are the marine Temblor Formation of Dickinson (1966a, 1966b), which is composed of semifriable arkosic sandstone, gray claystone, and local basal conglomerate. The unit lies unconformably on formations ranging from Eocene to Franciscan, with increasing discordance westward toward the San Andreas fault. In most places it is a few hundred feet thick, although in parts of the Temblor Range it may be either absent or as much as 4,000 feet thick. Southwest of the San Andreas fault, this unit is represented by terrestrial red conglomerate exposed only in the Red Hills. It is as thick as 3,000 feet and is composed of unsorted granitic cobbles and boulders in a matrix of red to gray arkosic sandstone. It here rests directly on granodiorite. About 3,200 feet of similar conglomerate was pentrated in an exploratory well (No. 20 on pl. 1 and in table 3) 2 miles northwest of Cholame. Several wells (Nos. 18, 31, 39, 40, 42) southwest and northwest of Shandon passed from Monterey Shale into a few hundred feet of marine sandstone of the Vaqueros Formation and terrestrial red beds, then into granitic basement.

The average density assumed for the lower Miocene rocks within the map area is 2.4 g/cm^3, although local variations from this value are common.

MONTEREY SHALE

The Monterey Shale is a distinctive unit of marine siliceous shale of early, middle, and late Miocene age. It is present on both sides of the San Andreas fault, but the stratigraphy of the northeast side differs from that of the southwest. Northeast of the fault, it is exposed in the Temblor and Diablo Ranges. It is as thick as 4,000 feet in the Temblor Range near Bitterwater Creek but thins northward to only 600 feet in McLure Valley. In the Bitterwater Creek area, the Monterey Shale is composed of three members, in ascending order: (1) Gould Shale Member, siliceous shale, about 600 feet thick, lower and middle Miocene, (2) Devilwater Shale Member, clay shale and siltstone, about 1,000 feet thick, middle Miocene, and (3) McLure Shale Member, siliceous shale, 2,500 feet thick, middle and upper Miocene. The Gould Shale Member is present only in the Temblor Range where the member extends southeastward from Franciscan Creek. The Devilwater Shale Member persists through much of the Temblor Range and northwestward to Turkey Flat. In much of the Shale Hills of the Temblor Range and McLure Valley, these two lower members are absent. The McLure Shale Member persists throughout the Temblor and Diablo Ranges but is only about 600 feet thick in the Diablo Range.

Southwest of the San Andreas fault the Monterey Shale is not exposed within the mapped area but is present in the subsurface. Exploratory wells drilled

for oil or gas southwest and west of Shandon (Nos. 32, 39, 40, 41, and 42 on pl. 1 and in table 3) passed through more than 1,000 feet of Monterey Shale between sandstones of the Santa Margarita and Vaqueros Formations. Northeastward this shale unit thins out at or near the San Juan fault. The Monterey Shale of this area is of middle Miocene age and is composed of a lower unit of argillaceous shale and an upper unit of siliceous shale.

The wet bulk density assumed for the Monterey Shale is 2.3 g/cm^3 in conformity with Clement's data (1965) from an area to the north. Dry bulk densities for this shale may be as low as 1.4 g/cm^3, as suggested by Byerly's data (1966).

UPPER MIOCENE AND PLIOCENE SEDIMENTARY ROCKS

Sedimentary rocks of late Miocene and Pliocene age are of different stratigraphy on opposite sides of the San Andreas fault. Northeast of the fault the sequence, in ascending order, consists of (1) the Reef Ridge Shale, 0 to 500 feet thick, uppermost Miocene, and (2) the Etchegoin Formation, interbedded marine sandstone, siltstone, and clay shale, 7,000 feet thick. In the Kettleman Hills the equivalent of the upper 2,000 feet of the Etchegoin Formation is mainly marine and brakish-water siltstone known as the San Joaquin Formation, upper Pliocene. (See Woodring and others, 1940.)

Southwest of the San Andreas fault, the sequence, in ascending order, consists of (1) the Santa Margarita Formation, a marine friable sandstone about 1,200 feet thick, upper Miocene and lower Pliocene(?), exposed in the Red Hills and northwest of Cholame, (2) Pancho Rico Formation, diatomaceous mudstone, as thick as 1,200 feet, lower Pliocene, exposed west of Cholame Valley only, (3) unnamed sandstone and siltstone, Pliocene(?), as much as 2,000 feet thick in wells northwest and southwest of Shandon only, and (4) Morales(?) Formation, terrestrial gravel and sand, 0 to 700 feet thick, upper Pliocene(?).

Average bulk densities used for gravity interpretation range from 2.2 to 2.3 g/cm^3, slightly less than the assumed average wet bulk density of the Monterey Shale.

UPPER CENOZOIC VALLEY DEPOSITS

Alluvial and lacustrine sedimentary deposits of late Pliocene and Pleistocene age are extensive on both sides of the San Andreas fault. The sediments are weakly consolidated gravels, sands, clays, and thin marl beds having an aggregate thickness of as much as 3,000 feet. Those deposited in the San Joaquin Valley region east of the Diablo and Temblor Ranges are known as the Tulare Formation. They lie conformably on Pliocene marine deposits north of McLure Valley, and unconformably on older rock units south of that valley. They were derived largely from the Diablo and Temblor Range uplifts. The sediments deposited in the upper Salinas Valley region west of the Diablo and Temblor Ranges are known as the Paso Robles Formation, which lies unconformably on Pliocene and Miocene formations. The Paso Robles Formation was derived largely from the Santa Lucia and La Panza Ranges to the southwest and the Temblor and Diablo Ranges to the northeast. On the basis of a heavy-mineral study in the Paso Robles Formation, Galehouse (1967) suggested right-lateral movement on the San Andreas fault of approximately 25 miles since Paso Robles deposition.

Bulk densities of the valley deposits assume a broad spectrum of values depending upon whether or not the materials are water-saturated. In the present study, an average wet bulk density of 2.2 g/cm^3 was assumed.

SURFICIAL DEPOSITS

Surficial deposits include alluvium of Pleistocene and Holocene age and landslide debris. The alluvium is composed of unconsolidated gravel, sand, and clay. Much of the older alluvium covers the floors of major valleys to depths of perhaps 200 feet. Much of the more recent alluvium is found along streambeds and as flood-plain deposits. Landslide debris is very common and covers large areas, particularly on the west flank of Table Mountain. Surficial deposits are not shown on the geologic map at places where they are small in extent and the identity of the underlying rock unit is relatively certain.

Assumed wet and dry bulk densities for these various surficial deposits range from 1.4 to 2.0 g/cm^3.

GEOLOGIC STRUCTURE AND TECTONICS

STRUCTURAL SETTING

By far the most significant structural feature in the area is the San Andreas fault. The style of deformation throughout the area in fact may be related to the fault, with the intensity of deformation decreasing away from the fault. The same general structural pattern prevails on both sides of the fault, although deformation was considerably less intense in rocks overlying the relatively competent plutonic and metamorphic basement to the south-

west and more intense in rocks overlying more plastic Franciscan and ultramafic rocks to the northeast.

The area northeast of the San Andreas fault was intensely squeezed and the Diablo and Temblor Ranges were thereby elevated by compressive forces. The prevasively sheared and brecciated Franciscan and ultramafic rocks reacted to stress as a plastic mass would, and the overlying sedimentary rocks reacted as a crust. The formations are compressed into folds with axes that trend on the average about N. 50° W., compared with N. 40° W. for the San Andreas fault. The folds are most severely compressed adjacent to or near the fault and progressively less compressed and less crowded away from the fault. This fold pattern appears to be the effect of lateral drag, which resulted from southeastward movement of the area northeast of the San Andreas fault relative to the Salinian block and which combined with severe pressure of rigid Salinian basement rocks against the more pliable terrane of Franciscan and utramafic rocks northeast of the fault.

The Salinian block was much less deformed than the area northeast of the fault because its plutonic and metamorphic basement was more resistant to stresses. As a consequence, the overlying sedimentary cover, which is much thinner than that northeast of the San Andreas fault, is generally undeformed. Only within a few miles of the San Andreas fault are sedimentary rocks mildly deformed into minor folds, which, like folds northeast of the faults, have axes that trend about N. 50° W.

STRUCTURAL HISTORY

The mapped area was affected by diastrophism during the following times: (1) early Cretaceous (?), (2) Paleocene, (3) Oligocene, (4) late Pliocene to early Pleistocene, and (5) late Pleistocene.

The granitic rocks of the Salinian block were emplaced in the metamorphic rocks during Cretaceous time according to the age determination of Evernden and others (1964). Other plutonic rocks, such as the hornblende quartz gabbro of Gold Hill, were emplaced earlier.

It is not definitely known where or how the Franciscan rocks became pervasively sheared and brecciated. The ultramafic rocks were emplaced during or after their deposition and are themselves sheared and brecciated. The lack of such deformation in the overlying Cretaceous and Tertiary rocks suggests that the shearing took place before these rocks were deposited, that is, presumably in early Cretaceous or very late Jurassic time.

The unconformity at the base of the Eocene marine sedminentary sequence of the area northeast of the San Andreas fault indicates mild deformation, uplift, and erosion after late Cretaceous time and before middle Eocene time, that is, probably in Paleocene or early Eocene time.

Severe diastrophism probably affected the whole area during Oligocene time. In the area northeast of the San Andreas fault, this disturbance is indicated by the great unconformity at the base of the Miocene rocks and by the westward overlap or progressively older formations toward the San Andreas fault. During this diastrophism the Franciscan and ultramafic rocks were exposed, probably for the first time, near and adjacent to the San Andreas fault by regional northeastward tilting and folding. Southwest of the San Andreas fault, the crystalline basement was probably stripped bare of any overlying sedimentary rocks that may have been present, then covered by Oligocene and Miocene sediments.

The mapped area was affected by severe diastrophism at the end of Pliocene or beginning of Pleistocene time, as indicated by the great unconformity at the base of the Paso Robles and Tulare Formations. This diastrophism resulted in the first uplift of the present Diablo and Temblor Ranges, during which uplift the major folds that had formed in Franciscan rocks, Cretaceous rocks, and Eocene rocks during the Oligocene diastrophism were further compressed and perhaps faulted and many new folds in the Miocene and Pliocene sedimentary rocks were formed.

The diastrophism that began at the end of the Pliocene, if not locally continuous through Pleistocene time, was rejuvenated in late Pleistocene time after deposition of the Paso Robles and Tulare Formations. It resulted in uplift of the Diablo and Temblor Ranges to their present heights, further compression of folds formed during the Oligocene diastrophism, and formation of new folds, such as in the Kettleman Hills anticline, in the valley deposits. Most of the faults of this region probably formed during this and the Oligocene diastrophism.

The axes of folds as well as the traces of associated thrust faults formed during the Cenozoic diastrophic events have an average trend of about N. 50° W., which indicates that these structures must have been formed by the same stress. Many of the north- to northwest-trending faults show evidence of right-lateral displacement. The structural pattern of this region strongly suggests that the folds and

faults are genetically related to, and possibly subsidiary to, right-lateral movement on the San Andreas fault and were formed by the same stress or stresses, as postulated by Hill and Dibblee (1953). If this is so, the San Andreas fault must have been active during all the Cenozoic diastrophic events, if not continuously during Cenozoic time.

Thus nearly all structural features of the area may be directly or indirectly related to movement on the San Andreas fault. Abundant evidence within the mapped area and elsewhere indicates many tens of miles of right-lateral movement along the fault in Cenozoic time, as noted by Hill and Dibblee (1953) and Dibblee (1966).

DIABLO RANGE

The Diablo Range within the mapped area is composed of two southeastward-plunging anticlines separated by a syncline. The southwestern margin of the range is essentially an uplift on a major northeast-dipping reverse fault. The core of pervasively sheared Franciscan and ultramafic rocks exposed along the anticlinal uplift north of Castle Mountain and along Table Mountain is the southeastward continuation of the 30-mile-long exposure of these rocks along the northeast side of the San Andreas fault. (See Jennings and Strand, 1958.) The northeast anticline, referred to here as the Pyramid Hills anticline because it plunges southeastward into the Pyramid Hills, has a steep northeast flank, part of which has been displaced southeastward relative to the southwest flank, along a fault near the fold axis.

The Castle Mountain syncline, which forms the prominent feature of Castle Mountain, plunges eastward and is offset northward on a fault from the McLure Valley syncline, its southeastward continuation.

The Franciscan rocks of Table Mountain are partly overlain by remnants of a thrust(?) plate of Cretaceous sedimentary rocks, as mapped by Dickinson (1966a, 1966b). Along the crest of this mountain both of these rocks are partly covered by a body of serpentinite that was mapped and described by Dickinson (1966a) as a subhorizontal sheet about 12 miles long which was extruded by plastic flowage from narrow, steeply-dipping dikes of serpentine breccia. Dickinson postulated that these dikes were fissure feeders, possibly along faults, that extended upward from a subterranean mass of serpentinite mobilized into cold plastic material by stresses during the Pliocene and Pleistocene orogenesis of the Diablo Range.

Southeastward, the pervasively sheared Franciscan and ultramafic rocks are covered by the Cretaceous marine sedimentary sequence, and the anticlinal structure terminates in a syncline in Cottonwood Canyon.

The northeastward-dipping Cretaceous section of Orchard Peak was elevated on the northeast-dipping reverse fault along which the southern Diablo Range was elevated. Scattered well data in the adjacent part of Antelope Valley suggest that the Cretaceous rocks of the foothills were elevated on another reverse fault against Miocene rocks to the south.

PARKFIELD-TURKEY FLAT AREA

The structure of the foothills southwest of the Diablo Range uplift is essentially that of a syncline that trends northwest through Turkey Flat. This structural feature involves Pliocene and Miocene sediments that overlie Lower(?) Cretaceous and Franciscan rocks, and to the southeast it becomes one of several small folds, cut and displaced right-laterally by many north-trending faults.

TEMBLOR RANGE

The northwestern Temblor Range within the mapped area is structurally complex. The Miocene rocks, which lie unconformably on Cretaceous and Franciscan rocks, are compressed into many northwest-trending folds. The Cretaceous rocks dip regionally to the northeast and are locally folded. The Franciscan and ultramafic rocks, with some mixtures of Cretaceous rocks, appear to be present adjacent to the San Andreas fault for an extent of possibly 23 miles but are in large part concealed beneath a thin cover of the Paso Robles Formation. The exposed parts of these pervasively sheared rocks include large masses of serpentinite, and an unknown amount of this rock may be concealed by the Paso Robles Formation.

GOLD HILL AREA

Exposures of crystalline basement rocks at and near Gold Hill and northwest of Parkfield are unconformably overlain by Eocene(?) rocks. All these rocks form a fault slice as wide as 2 miles on the northeast side of the San Andreas fault, dissimilar to any other rocks in the mapped area northeast of the San Andreas fault. The basement rocks are generally similar to those southwest of the San Andreas fault, but rocks of Eocene age are not known to occur southwest of the fault within the mapped area. As the Gold Hill fault that bounds this slice on the northeast is exposed at few places, its char-

acter is not definitely known. East of Gold Hill, it appears to be a near-vertical zone of gouge as wide as 15 feet. There is no indication of any activity on this fault, and it appears to have been long dead. This slice may have been emplaced in middle or late Tertiary time.

SOUTHWEST OF SAN ANDREAS FAULT

The area southwest of the San Andreas fault is deformed within a few miles of the fault and near the San Juan fault. Northwest of Cholame the Miocene rocks are gently compressed into folds whose axes trend about N. 50° W. The unconformably overlying Paso Robles Formation is, within 3 miles of the San Andreas fault, deformed into many minor folds with axes of similar trend. All these folds must have formed by right-lateral drag on the San Andreas fault.

The only major fault within the Salinian block in the mapped area is the San Juan fault which, in the Red Hills uplift on the east side of the fault, exposes granitic basement and overlying Miocene rocks. This fault extends southward for many miles. Northward it disappears below the Paso Robles Formation, but an en echelon alinement of northwest-trending minor folds in that formation suggests a continuation of the fault below the Paso Robles. These and other minor folds associated with the San Juan fault suggest that movement on this fault also is right lateral. As will be noted in a later section, gravity data suggest that a prominent subsurface fault may extend from the exposed San Juan fault at the Red Hills uplift southeastward to the San Andreas fault near the southeastern corner of the mapped area.

GRAVITY AND MAGNETIC FEATURES

GENERAL PATTERNS

GRAVITY TRENDS

The gravity field in the mapped area is characterized by a regional gradient of about 2 mgal per mile which decreases toward the northeast and is interrupted by a broad gravity high northeast of the San Andreas fault near Cholame. Smaller perturbations of the regional field occur northeast of the fault as anomalies near Table Mountain, the Kettleman Plain, Palo Prieto Pass, and Bitterwater Valley and southwest of the fault near Red Hills, San Juan Valley, and the Estrella River valley. The northeastward decrease of the regional field may be caused partly by a northeastward thickening of the continental crust, perhaps coupled with a northeastward decrease in average density of the lower continental crust and upper mantle, as proposed by Thompson and Talwani (1964) for an area to the north. However, part of what would ordinarily be considered the regional field is attributed to large anomalous concentrations of high- or low-density masses within the upper 10 miles of the crust.

MAGNETIC TRENDS

The magnetic field within the area studied is characterized by two conspicuous positive anomalies: (1) a narrow elongate high that trends nearly parallel to Table Mountain over much of its extent, and (2) a broad elliptical high that spans the San Andreas fault near Palo Prieto Pass (pl. 2). Each of the positive anomalies has an associated polarization low developed over relatively nonmagnetic terrane to the north. The anomalies are superposed on a regional field that increases uniformly toward the north-northeast. Coast and Geodetic Survey charts indicate that the gradient of this regional field as estimated from the aeromagnetic map is greater than that attributable to the dipolar component of the earth's field by about 5 gammas per mile in a northeast direction. This residual gradient, if due to interpolation uncertainty resulting from use of small-scale charts, may reflect an average northeastward increase in magnetization of that part of the earth's lower crust above the Curie isotherm. The dipolar regional field of 9 gammas per mile increasing north-northeastward has been removed from plate 2.

ANOMALIES NORTHEAST OF SAN ANDREAS FAULT

GRAVITY HIGH AT CHOLAME VALLEY

The salient feature of the gravity map is a broad high northeast of the San Andreas fault that peaks about 7 miles north-northwest of Cholame. This feature consists of a 10-mgal doublet covering some 40 square miles superposed on a much broader 20-mgal high covering perhaps 300 square miles. The anomaly is associated with a terrane of Franciscan rocks, intruded in part by ultramafic rocks, and overlying Cretaceous miogeosynclinal rocks. This terrane is covered in places by sedimentary rocks.

Although the principal source of the gravity high appears to be a combination of Franciscan and miogeosynclinal Cretaceous rocks in contact with lower density sedimentary rocks to the northeast and southwest, the configuration of the anomaly is probably much influenced by subsurface serpentinites and slightly influenced by a single plutonic rock sliver and folded sedimentary rocks. The highest part

of the anomaly north-northwest of Cholame is associated primarily with serpentine-deficient Franciscan rocks similar to those associated with a major positive gravity anomaly northwest of Panoche Valley in the Diablo Range, about 60 miles northwest of the mapped area. (See Bishop and Chapman, 1967.) The decrease in gravity at the northeastern flank of the anomaly is largely caused by a thick northeast-dipping sequence of miogeosynclinal Cretaceous rocks and overlying lower density Cenozoic rocks. The steep southwestern flank of the anomaly is produced by a combination of Franciscan rocks northeast of the San Andreas fault in contact with granitic rocks of similar density overlain by low-density rocks of the Paso Robles Formation southwest of the fault.

One possible subsurface density profile across the gravity high at Cholame Valley is shown in generalized form in figure 2. The computed anomaly associated with the idealized density section compares favorably, though approximately, in shape and amplitude with the observed anomaly. It will be noted that density units used in figure 2 and elsewhere in the report need not correspond uniquely to particular stratigraphic units. For example, in figure 2, Franciscan rocks and Salinian basement rocks adjacent to the San Andreas fault are interpreted to have identical average densities; farther southeast, Franciscan rocks are interpreted to have

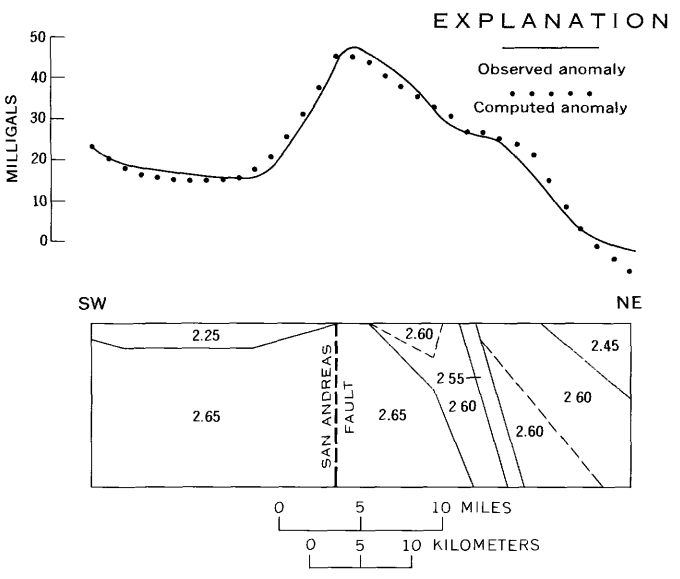

FIGURE 2.—Comparison of computed gravity anomaly of a two-dimensional model with observed Bouguer gravity anomaly near Cholame Valley. Strike of model is N. 40° W. Gravity datum is arbitrary. Line of section corresponds approximately to profile *A–A′* of plate 4.

an average density 0.05 g/cm^3 greater than that of Salinian basement rocks.

The configuration of the gravity high appears to be strongly controlled on the north and south by two major subsurface accumulations of serpentinite, as interpreted on the basis of positive magnetic anomalies. At the northern flank of the high near Table Mountain, an inferred steeply dipping tabular serpentinite mass below exposed serpentinites and tectonic breccia produces a shallow negative gravity trough. Southeast of Cholame the southeastern flank of the Cholame high is depressed, though somewhat less conspicuously, about 4 miles north of Palo Prieto Pass, where magnetic data suggest a deeply buried magnetic mass. In the absence of these lower density subsurface masses, the Cholame high would appear as an asymmetrical northwest-trending gravity ridge, approximately parallel to the outcrop pattern of Franciscan and miogeosynclinal Cretaceous rocks in the area.

The doublet configuration of the highest part of the gravity anomaly may be attributed in part to the gabbro of Gold Hill and to the serpentinite along the Gold Hill fault. The plutonic rock at Gold Hill is as much as 0.2 to 0.5 g/cm^3 denser than most surrounding rocks, and this density contrast probably contributes significantly to the local gravity peak at Gold Hill. The intervening gravity saddle to the southeast may be caused in part by the serpentinized ultramafic rocks cropping out along the Gold Hill fault between the local gravity peaks. Both gravity and magnetic data indicate that the subsurface volume of these ultramafic rocks is small. The southeastern local peak may be interpreted as a relative high associated with Franciscan rocks in contact with serpentinized ultramafic rocks and folded Cenozoic sedimentary rocks. Other relative highs associated with Franciscan or miogeosynclinal Cretaceous rocks, in places partly covered by Cenozoic sedimentary rocks, are the segmented gravity ridge immediately northeast of Table Mountain, the local positive gravity anomalies west and northwest of Antelope Valley, and the gravity ridges north and west of Bitterwater Valley.

An idealized cross section through the center of the gravity high at Cholame Valley is shown as profile *A–A′* on plate 4.

ANOMALIES AT TABLE MOUNTAIN

A relatively narrow, arcuate magnetic ridge that trends parallel to and northeast of the San Andreas fault at the northwest corner of the mapped area (pl. 2) bends east-southeastward northeast of Park-

field to follow the trend of Table Mountain. This anomaly, about 150 gammas in amplitude at a level 0.6 mile above mean topography, has a symmetry axis slightly south of the Table Mountain ridge line, which terminates near the extinction of the ultramafic outcrop belt 10 miles east of Parkfield. The position of the elongate magnetic high is thus somewhat south of the elongate gravity low, which is more directly centered over the Table Mountain ridge axis, although both anomalies presumably are generated by a common source. It is clear that both features are associated over their entire extent with highly serpentinized ultramafic rocks, as described by Dickinson (1966a), and that their subsurface source is serpentine-rich rocks.

The shape of the magnetic anomaly precludes the possibility that the main part of the source is a vertical tabular body, provided that total magnetization nearly parallel to the earth's ambient magnetic field is assumed. Rather, the anomaly is consistent with that produced by a tabular source that dips northward to northeastward. Because the effect of remanent magnetization on the direction of total magnetization is unknown, interpretation of the magnetic source relies significantly on the Bouguer gravity data (pl. 1).

Observed aeromagnetic and gravity profiles extending from Gold Hill northward to lat 36° 00′ N., long 120° 20′ W. across the magnetic high and gravity low at Table Mountain are shown in figure 3*A*, *B*, and *C* with computed anomalies of various models. Both the magnetic and gravity anomalies of the vertical tabular model shown in Figure 3*A* are inconsistent with the shapes of observed anomalies. Figure 3*C* indicates that if a vertical-sided model is invoked as a magnetic source at depth, it must be accompanied by a north-dipping tabular body adjacent to it. A single north-dipping body, shown in Figure 3*B* generates magnetic and gravity anomalies similar to those observed. The top of this model, however, is probably deeper than the top of most of the material of the actual magnetic source, and assumptions of model magnetization and density contrasts are probably higher than those of the actual source.

Two points must be made about the gravity anomalies. First, the observed gravity anomaly can be considered a nearly symmetrical low by subtracting a linear regional field from the original anomaly and interpreting this regional field in terms of lateral thickening of the earth's lower crust and lateral uniform changes in density in the earth's lower crust or upper mantle. Part of the regional field should undoubtedly be interpreted in this fashion. However, it seems compelling to postulate that many relatively broad gravity gradients, such as the gradient of the observed gravity anomaly at Table Mountain, are caused by anomalous concentrations or deficiencies of mass of considerable size within the upper 10 miles of the earth's crust. The evidence here seems especially convincing, for a vertical-sided body generating a symmetrical gravity low would have to assume a shallow magnetization inclination to match the symmetry of the observed magnetic feature. The magnetic anomaly peak of such a model, though nearly symmetrical, would be displaced considerably southward from the observed magnetic anomaly peak, assuming the computed and observed gravity anomalies are horizontally registered. Second, the abrupt rise of the gravity anomaly at the south end of the profile is attributable in part to the dense hornblende quartz gabbro body of Gold Hill. Computed anomalies for models should therefore have a southern gradient somewhat lower than that of the observed anomaly, as is the case for models in figure 3*A*, *B*, and *C*.

As additional information in interpreting the anomaly source at Table Mountain, aeromagnetic data along the single transverse flight line through the study area are shown in figure 3*D*. The path of this line, shown on plate 2, passes approximately 2 miles northwest of Gold Hill and intersects the easternmost part of Table Mountain. A model that satisfies the anomaly requirements for the magnetic source along this profile is a tabular body 2 to 2½ miles thick that crops out at ground surface and dips 75° NE. to a depth of about 10 miles, with a total magnetization contrast of 0.0005 emu/cm^3. The magnetic and gravity data collectively indicate that the magnetic source of the anomaly at Table

FIGURE 3.—Comparison of computed total-intensity magnetic and gravity anomalies of two-dimensional models *A*, *B*, and *C* with observed aeromagnetic and Bouguer gravity anomalies at Table Mountain, and comparison of computed total-intensity anomaly of two-dimensional model *D* with aeromagnetic anomaly along the single transverse flight line across Table Mountain. Strike of models *A*, *B*, and *C* is parallel to magnetic north; strike of model *D* is N. 45° W. Assumed magnetization inclination is 60°. Positive numbers refer to total magnetization intensity contrasts in emu/cm^3; negative numbers in parentheses, to density contrasts in g/cm^3. Datum levels of anomalies are arbitrary. Data of model *D* along observed profile were taken directly from magnetic tape, independent of contoured map. (See facing page.)

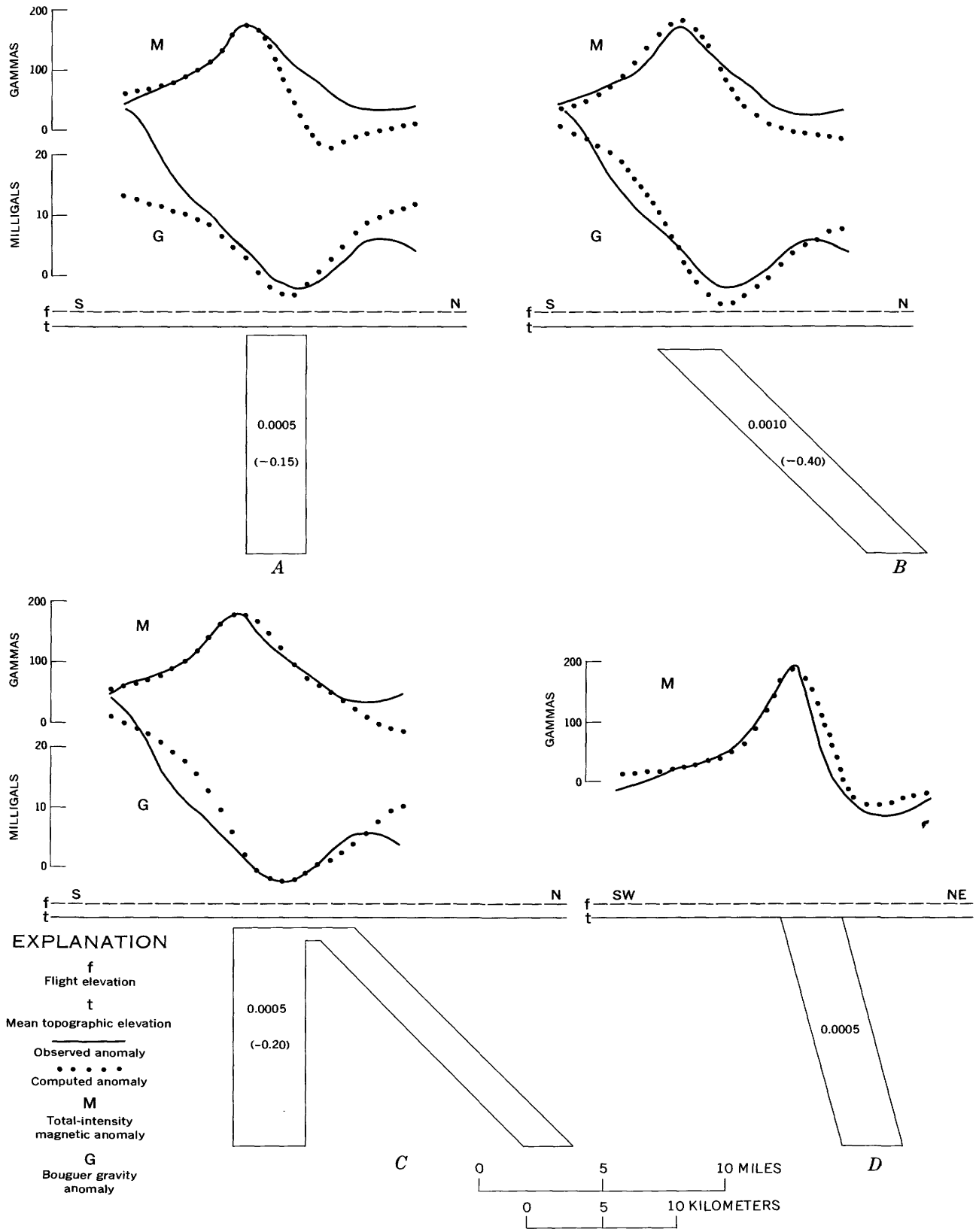
GAMMAS
200
100
0
MILLIGALS
20
10
0
M
G
f
t
S
N
0.0005
(−0.15)
A
0.0010
(−0.40)
B
SW
NE
0.0005
(−0.20)
C
0.0005
D
EXPLANATION
f
Flight elevation
t
Mean topographic elevation
Observed anomaly
Computed anomaly
M
Total-intensity magnetic anomaly
G
Bouguer gravity anomaly
0
5
10 MILES
0
5
10 KILOMETERS

Mountain is about 2½ miles thick over most of its extent, dips 45° to 75° northward to northeastward with the dip steepening along strike toward the east, has a roof that for the main part of the mass is from 0 to ½ mile deep and a floor possibly 10 miles deep, and has an average negative density contrast with surrounding rocks of about −0.25 g/cm^3 and an average total magnetization intensity contrast with surrounding rocks of 0.0005 to 0.0010 emu/cm^3.

We may note that the nearly vertical narrow fissure feeder of the serpentinite extrusion described by Dickinson (1966a) probably extends no more than 1,000 or 2,000 feet deep before it connects with the thicker north-dipping trunk body. Furthermore, the density and magnetization parameters obtained from model studies probably apply to mass and magnetic sources consisting of various amounts of serpentinite intermixed with brecciated Franciscan rocks. The degree of serpentization, and consequently the density and magnetization contrast, may depend significantly on depth, a parameter not considered in the modeling.

MAGNETIC HIGH AT PALO PRIETO PASS

The largest known magnetic anomaly along the San Andreas fault (in terms of amplitude and areal extent) is situated close to the fault trace southeast of Cholame, near Palo Prieto Pass. The total-intensity anomaly, delineated by five out of seven longitudinal flight lines in the reconnaissance survey, reaches a maximum of 400 gammas at an elevation of 0.85 mile above mean land-surface altitude. The anomaly is approximately elliptical in plan view, with its major axis alined along the fault trace. The feature, as contoured from the aeromagnetic data, extends for approximately 8 miles on either side of the fault and for about 20 miles along the fault.

The location of part of the anomaly at Palo Prieto Pass directly over the fault trace suggests the possibility of a single subsurface source which partly transects the fault or, alternatively, a compound source of materials which occur on opposite sides of the fault and are fortuitously adjacent to one another in the subsurface. As an aid to understanding possible locations of the buried magnetic source rocks relative to their associated anomaly, total-field anomalies of eight magnetic models are compared with the observed magnetic anomaly in figure 4. It may be noted that models striking 45° W. of magnetic north and having a magnetization inclination of 60° generate magnetic anomalies that are centered south of the plan-view centers of the models.

Comparison of anomalies produced by models with identical volumes, magnetizations, and depths of burial (fig. 4*A*, *B*, *C*) indicates that the symmetry of the computed anomaly depends on the dip of these bodies. Anomalies shown in figure 4*A* and *B* appear to have northeast gradients greater than the gradient associated with the observed anomaly. Thus, in figure 4*A* the southwest-dipping dike bounded by a hypothetical southwest-dipping San Andreas fault and in figure 4*B* the vertical prism bounded by a hypothetical vertical fault may be tentatively dismissed as probable sources on the basis of anomaly symmetry. The northeast-dipping dike of figure 4*C* and the trapezoidal cross-section models of 4*D*, *E*, *F*, *G*, and H generate anomalies similar in shape to the observed anomaly.

Vertical-intensity ground magnetic data over the southeastern part of the mapped area (pl. 3) generally confirm the shape, amplitude, and areal extent of the anomaly at Palo Prieto Pass but define its location more precisely than the aeromagnetic data. The vertical-field anomaly is about 500 gammas in amplitude, with a few local spikes of more than 1,000 gammas (not contoured), and its major axis is displaced 1 to 2 miles northeast of the aeromagnetic anomaly axis, which is coincident with the San Andreas fault. A small part of the northeastward displacement of the vertical-field anomaly relative to the total-field anomaly is to be expected on the basis of theoretical calculations of magnetic field components generated by sources magnetized parallel to the earth's magnetic field in the area. This displacement may be seen for computed anomalies of total- and vertical-field intensity of given models shown in figures 5 and 7 and discussed below. The remainder of the anomaly shift is an expression of the more accurate location of the vertical-field anomaly, which was contoured on the basis of data more densely and uniformly distributed than the aeromagnetic data.

A more detailed inspection of plate 3 suggests

FIGURE 4.—Comparison of computed total-intensity magnetic anomalies of three-dimensional models *A* through *H* with observed aeromagnetic anomaly at Palo Prieto Pass. Horizontal lines of model cross sections represent flight-line elevation. Models are composed of rectangular parallelepipeds shown as dashed lines. Assumed magnetization inclination is 60°. Numbers refer to total magnetization intensity contrasts in emu/cm^3.

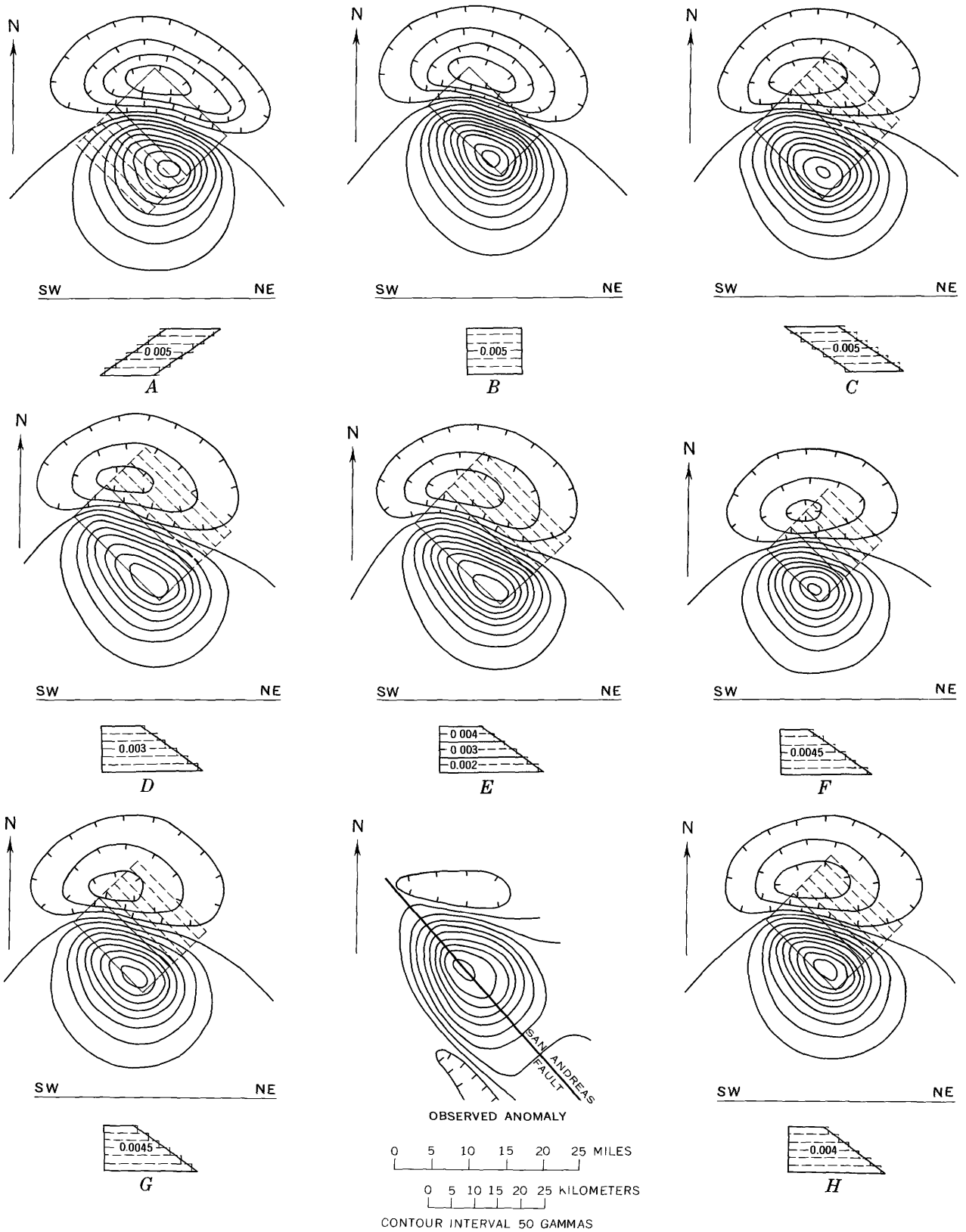
N
SW
NE
0.005
A
0.005
B
0.005
C
0.003
D
0.004
0.003
0.002
E
0.0045
F
0.0045
G
SAN ANDREAS FAULT
OBSERVED ANOMALY
0 5 10 15 20 25 MILES
0 5 10 15 20 25 KILOMETERS
CONTOUR INTERVAL 50 GAMMAS
0.004
H

that the source of the observed anomaly has a plan-view strike length of approximately 13 miles, a total magnetization within the range of 0.002 to 0.005 emu/cm^3, a roof 4 to 6 miles wide and 2 to 3 miles below ground level, and a floor 10 to 12 miles wide and perhaps 8 to 10 miles below ground level (floor level would represent Curie isotherm level). It is evident that if the source material is magnetized approximately parallel to the earth's ambient field, the northeast periphery of the body must dip northeastward.

Because of the inherent lack of precision in the aeromagnetic contouring due to the wide spacing of flight lines and to the possible bias of the central flight line on the contouring, it is instructive to compare both total- and vertical-field anomalies of selected models with the observed anomalies. It should be noted that the aeromagnetic data and vertical-intensity ground magnetic data are independent of one another; both component anomalies must be satisfied by a given model that is to be considered analogous to the natural magnetic source.

Total- and vertical-field anomalies of eight models striking 45 ° W. of magnetic north and dipping northeastward are compared with the observed aeromagnetic and vertical-intensity ground magnetic anomalies in figure 5. Of the models shown, the simple trapezoidal cross-section form of figure 5*A* most closely satisfies both observed anomalies. The models in *B*, *C*, and *D* were constructed on the possibility that the magnetic source is serpentine-rich. The model in *B* represents a stratiform body that is more highly serpentinized on top than on the bottom owing to a gross decrease in water content with depth. The model in *C* simulates an originally fresh ultramafic body whose periphery has been serpentinized; the model in *D* combines the horizontal layering of *B* and the carapace of *C*. The models in *E*, *F*, *G*, and *H* of figure 5 represent, respectively, an asymmetrical anticlinal body, a bent tabular body, a thick dike, and a thin dike. It may be noted that it is possible to constrain more of the material of the models in *A*, *B*, *C*, and *D* northeast of the San Andreas fault (shown relative to the observed anomalies) than the models in *E* through *H*. For this reason the source of the anomaly at Palo Prieto Pass is postulated to be trapezoidal in cross section, with its southwest side abutting the vertical San Andreas fault and its northeast side dipping approximately 45° NE. Analyses of the models in *B*, *C*, and *D* and other relatively complex models not shown have indicated the facility of matching either the total- or vertical-field observed anomaly by choosing a suitable combination of physical parameters such as body geometry and magnetization distribution but have also indicated the difficulty of matching both anomalies with the observed ones. A simple, though suitable, source for the anomaly at Palo Prieto Pass shown in figure 4*A* is assumed to possess a uniform average total magnetization intensity contrast of 0.002 emu/cm^3. The roof of the source is taken to be 6 miles wide and 3 miles below ground surface; the floor of the source, 12 miles wide and 9 miles deep. It should be emphasized that the depth below ground level to the floor of the source can be much less accurately estimated than the depth to the top of the source because volumes of magnetic rock far from the magnetic field detector are not as strongly sensed as volumes closer to the detector. The location of the southwest edge of the model just southwest of the San Andreas fault reference line in figure 2*A* is considered to result from inherent uncertainty in the observed data and in the anomaly-matching process, which together may represent as much as half a mile of horizontal distance.

Although the model anomalies shown in figures 4 and 5 indicate that a possible source for the anomaly at Palo Prieto Pass may be constrained to the northeast side of the San Andreas fault, the geologic presence of the Red Hills uplift (pl. 1) southwest of the fault suggests the possibility that Salinian basement rocks may contribute significantly to the southwestern flank of the anomaly. Results of the ground magnetic survey, which in part covered the uplifted basement area, indicate that these plutonic and metamorphic rocks are not sufficiently magnetic to appreciably affect the observed anomaly. The relatively simple geometric configuration of the observed anomaly also suggests that it has a single magnetic source.

The source material for the anomaly at Palo Prieto Pass is not definitely known. Geologic mapping within the study area indicates that three rock types might be capable of possessing the requisite magnetization of 0.002 emu/cm^3: (1) plutonic rocks, found as blocks within the fault zone, as outcrops southwest of the fault, and in drill holes southwest of the fault, (2) mafic volcanic rocks, found in a small isolated outcrop within Tertiary sedimentary rocks northeast of the fault, and (3) serpentinites and associated ultramafic rocks, found as sheets and

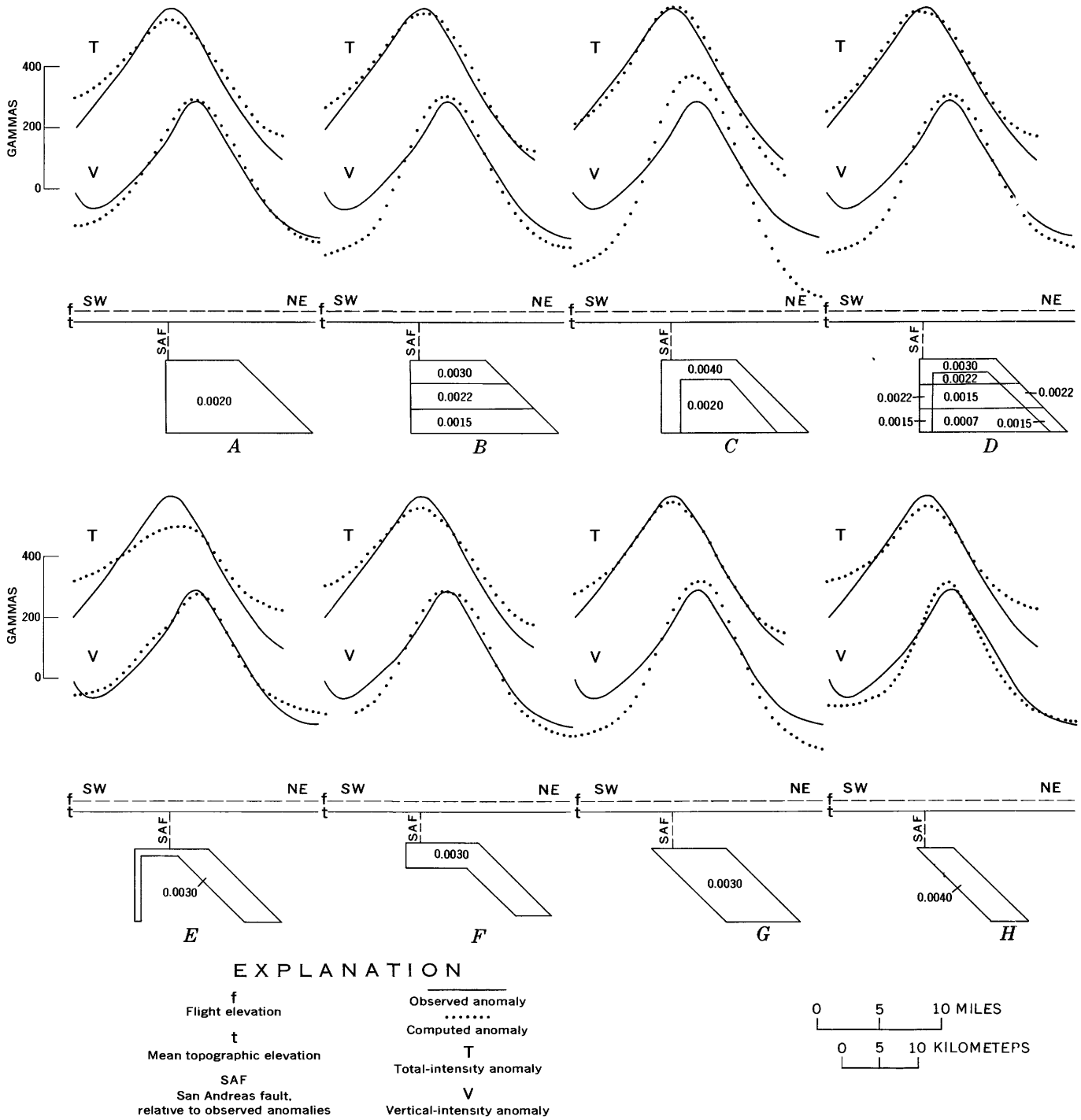

FIGURE 5.—Comparison of computed total- and vertical-intensity magnetic anomalies of three-dimensional models in *A* through *H* with observed aeromagnetic and ground magnetic anomalies at Palo Prieto Pass. Models strike N. 45° W. and have magnetization inclinations of 60°. Numbers refer to total magnetization intensity contrasts in emu/cm³. Datum levels of anomalies are arbitrary.

pods of limited outcrop extent northeast of the fault. Other rock types that might be magnetic enough to produce the anomaly, and found in Franciscan terrane to the north, are gabbro and spilitic

basalt. (See Grommé and Gluskoter, 1965; Griscom, 1966; Wentworth, 1968.)

Because the source of the anomaly is believed to be confined to the northeast side of the fault, samples of potentially magnetic rock types were collected for magnetic measurement along, and northeast of, the fault zone in the mapped area. Sampling sites are shown in figure 6. North of Cholame, sampling site numbers are prefixed by N, and the sites consist of six outcrops of serpentinite and one outcrop of hornblende quartz gabbro. South of Cholame, sampling site numbers are prefixed by S, and the sites consist of six outcrops of serpentinite and one outcrop of volcanic rock. Remanent magnetization was not measured because outcrops suitable for collecting oriented samples were absent in critical areas. Susceptibility measurements of powdered samples were made to establish possible limits on the induced magnetization of the anomaly source. Generalized results of the susceptibility results are summarized in table 4. The data indicate that (1) susceptibility values of serpentinite and associated ultramafic rocks are highly variable over relatively small volumes of rock at a single site, (2) susceptibility values of serpentinites and associated ultramafic rocks generally fall into two contrasting groups—one group of 1 to 4 $\times$ 10^{-3} emu/cm^3 and another of about 5 $\times$ 10^{-4} emu/cm^3, (3) quartz gabbro rocks at a single outcrop of Gold Hill have weak susceptibilities, about 10^{-4} emu/cm^3, and (4) volcanic rocks east of Palo Prieto Pass have weak susceptibilities, about 10^{-4} emu/cm^3.

TABLE 4.—*Summary of magnetic susceptibility data*

Sampling site	General rock type	Total number of samples	Number of samples with magnetic susceptibility (emu/cm^3) of—		
			$\leq 10^{-4}$	10^{-4} to 10^{-3}	$\geq 10^{-3}$
N1	Serpentinite	20	--	9	11
2	------- do -------	27	2	7	18
3	------- do -------	16	--	8	8
4	Quartz gabbro	13	12	--	1
5	Serpentinite	10	--	2	8
6	------- do -------	11	--	9	2
7	------- do -------	13	2	10	1
S1	------- do -------	11	6	2	3
2	------- do -------	10	--	2	8
3	------- do -------	12	4	7	1
4	------- do -------	14	8	6	--
5	------- do -------	8	--	7	1
6	------- do -------	13	--	6	7
7	Volcanic rock	10	10	--	--

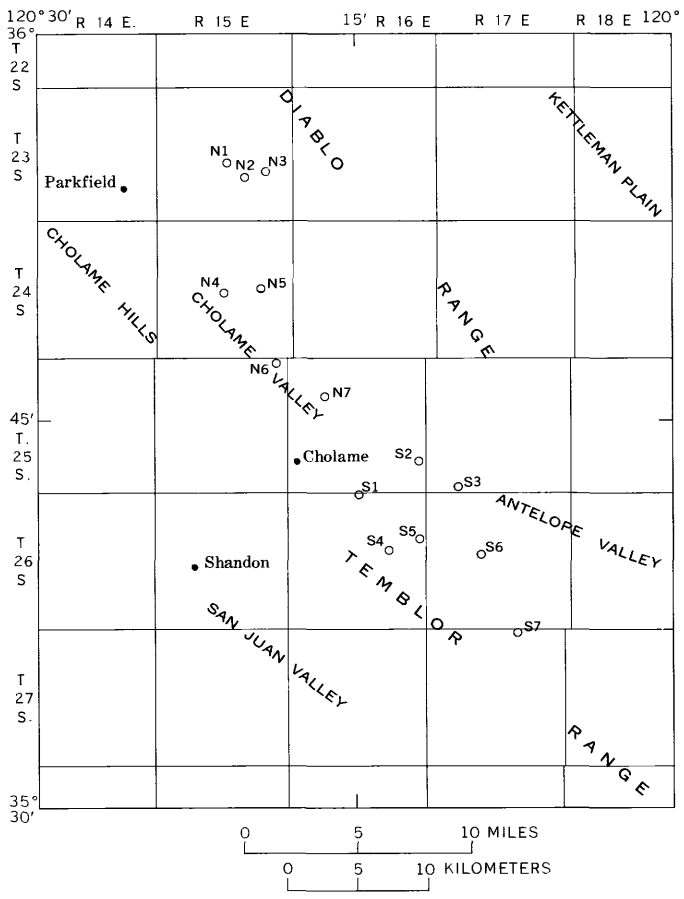

FIGURE 6.—Map showing sampling sites (large open circles).

It would appear that the occurrence of sporadic outcrops of ultramafic rocks and serpentinite just northeast of Palo Prieto Pass to a distance of 5 miles northeast of the fault, together with the susceptibility data, almost certainly points to an anomalous subsurface source of highly magnetic serpentinite. However, as seen on plate 2, outcrops of ultramafic rock and serpentinite such as those northeast of Cholame and southeast of Gold Hill have no aeromagnetic expression.

The single most important contribution to the analysis of the magnetic source at Palo Prieto Pass is the Bouguer gravity map. (See pl. 1.) In the area of the postulated subsurface body, the gravity field conspicuously flattens, which forms a shallow trough between Palo Prieto Pass and Polonio Pass, 5 miles to the north. Although part of the shallow depression is caused by Tertiary sedimentary rocks in a northwest-striking syncline, the broad flattening of the gravity field is attributed to deeper crustal rocks having an average density less than that of the Franciscan assemblage or the Cretaceous marine sedimentary sequence. Among the rock types considered as possible sources of the magnetic anomaly, gabbros and mafic volcanic rocks should have densities greater than, or at least equal to, the average Franciscan rock density, whereas serpentinite should have a density less than the average Franciscan rock density. Thus, we conclude that the most likely source of the magnetic anomaly at Palo

Prieto Pass is serpentinized ultramafic rock. Because of the probable high load pressures and limited amounts of sorbed water at the body's depth of burial, the average density is believed to be higher than the average density of serpentinites at Table Mountain. An idealized cross-sectional model across the San Andreas fault at Palo Prieto Pass is shown in figure 7, with observed and computed magnetic and gravity anomalies.

The susceptibility data further indicate that the required magnetization intensity of 0.002 emu/cm^3 can be realized by the induced magnetization alone of a number of serpentinite samples. Samples with susceptibilities exceeding 4×10^{-3} emu/cm^3 have more than enough induced magnetization to produce the anomaly at Palo Prieto Pass. If magnetization data of serpentinites at Burro Mountain (Burch, 1965) and Red Mountain (Saad, 1968) to the west and north of the study area are at least roughly applicable to serpentinites within the study area, the remanent magnetization intensity is less than the induced magnetization intensity, but probably by no more than a factor of two. Thus, in the two extremes of remanent magnetization parallel or antiparallel to the induced magnetization, susceptibilities of about 0.003 or 0.008 emu/cm^3 are required to produce the observed anomaly, assuming a remanent magnetization intensity of one-half of the induced magnetization intensity.

Remanent magnetization directions within the source rock may also be sufficiently random that considerable cancellation of magnetization occurs. If they are, the resultant remanent magnetization intensity over the volume of the body may be an order of magnitude less than the induced magnetization intensity. Further, the magnetic body may have obtained a viscous remanent magnetization parallel to the earth's ambient magnetic field. In either case, the total magnetization would assume a direction more nearly parallel to the earth's ambient field, thus validating the assumptions of total magnetization direction in the model studies. The occurrence of both highly random remanent magnetization directions over small rock volumes and viscous remanent magnetization have been reported by Burch (1965) and Saad (1968) in studies of California serpentinites.

An idealized cross section through the major magnetic anomaly at Palo Prieto Pass is shown as profile *B–B′* on plate 4. Why there are no great surficial accumulations of serpentinite in the Palo Prieto Pass area above the postulated subsurface body is not known. If, however, this mass was emplaced during Pliocene and Pleistocene time as postulated by Dickinson (1966a) for the Table Mountain body, possibly insufficient geologic time has elapsed for extensive diapiric intrusion of the subsurface material into loci of Pleistocene and Holocene faulting.

OTHER GRAVITY FEATURES

A conspicuous gravity trough over the Kettleman Plain near the northeast corner of the mapped area is associated with low-density Cenozoic sedimentary rocks in the Avenal syncline. Immediately northeast, the gravity field rises abruptly over the Kettleman Hills anticline. The amplitude of the negative anomaly over the Kettleman Plain suggests that dense Cretaceous rocks here may be as deep as 25,000 feet, perhaps about 10,000 feet deeper than similar rocks beneath the Kettleman Hills anticline. The gravity field continues to increase just northeast of the mapped area over domal structures in the Kettleman Hills. (See Boyd, 1948.)

The gravity map suggests that the exotic plutonic fault slice at Gold Hill, north of Cholame, has no appreciable subsurface extent northwest of the main exposed mass, where isolated fragments of other plutonic slices occur. The data indicate that, from Gold Hill northwest to serpentinite outcrops northwest of Table Mountain, average densities of rocks on opposite sides of the San Andreas fault are similar. A single narrow gravity ridge issues northwestward from the high at Cholame Valley, near Gold Hill, crosses the San Andreas fault, and continues about 12 miles northwestward out of the map area (Burch and Durham, 1970; Burch and others, 1971).

GRAVITY ANOMALIES SOUTHWEST OF SAN ANDREAS FAULT

The gravity map southwest of the San Andreas fault is characterized by a local high near Red Hills, a somewhat discontinuous trough near San Juan Valley, and a broad, slightly positive feature near the Estrella River valley.

The prominent local high centered 2 miles north of Red Hills is associated with an uplift of Salinian basement rocks on the northeast side of the San Juan fault. The amplitude of the anomaly suggests that the Salinian basement is vertically offset approximately 1 mile along the fault. The position of the anomaly peak about 2 miles north of Red Hills suggests that the Salinian basement may be anomalously dense beneath the sedimentary cover there. The southeasterly trend of the southern flank of the anomaly near Red Hills suggests that a subsurface

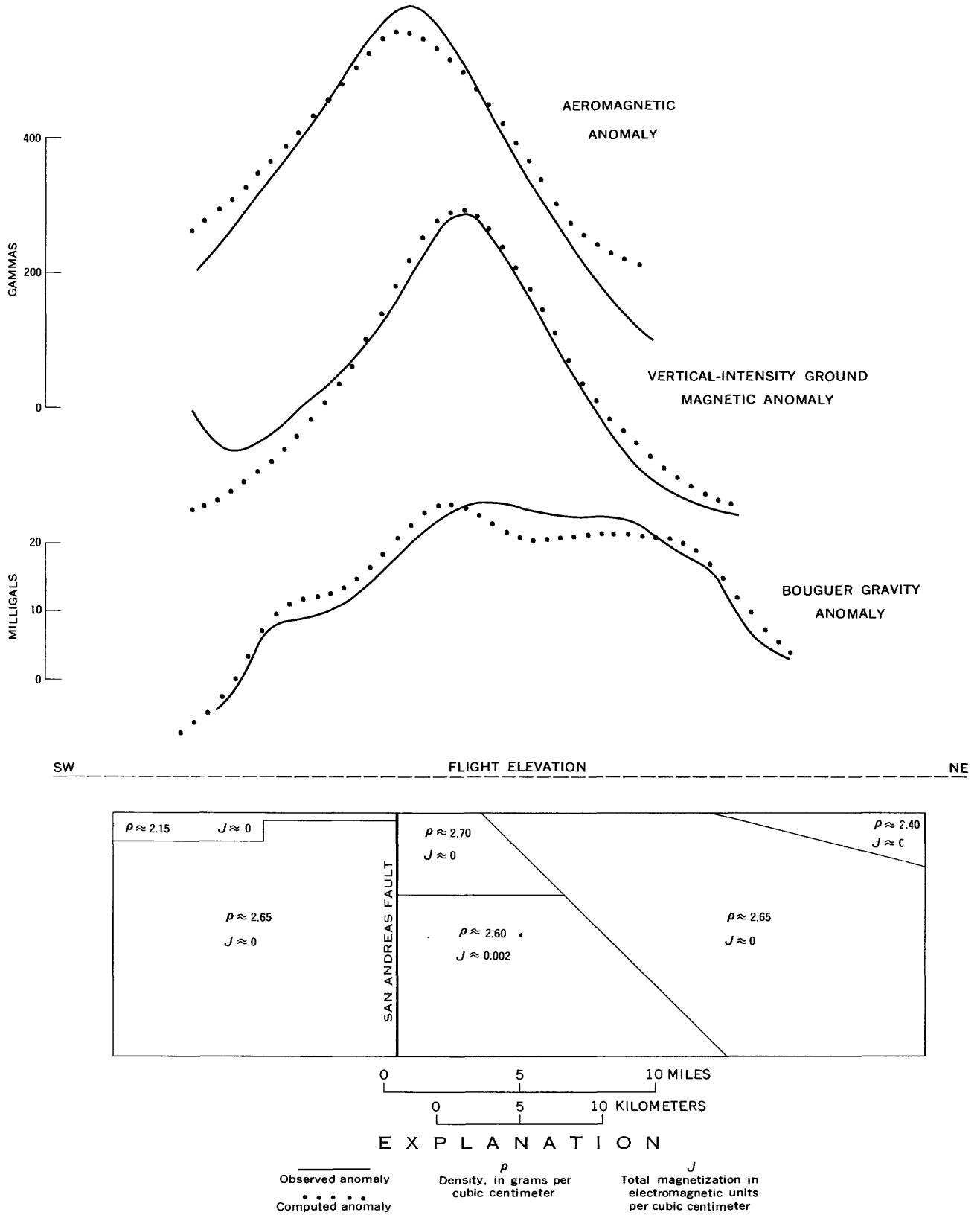

FIGURE 7.—Comparison of computed magnetic and gravity anomalies of a three-dimensional model having a strike length of 13 miles with observed anomalies at Palo Prieto Pass. Strike of model is N. 45° W. and magnetization inclination is 60°. Magnetic and gravity datums are arbitrary. Line of section corresponds approximately to profile *B–B′* of plate 4.

basement discontinuity may intersect both the San Juan and San Andreas faults near the southern end of the mapped area.

The lowest gravity values southwest of the San Andreas fault are within a discontinuous northwest-trending trough associated with low-density Cenozoic sedimentary rocks and deposits near San Juan Valley. This trough passes 1½ miles east of Shandon and turns abruptly west-southwest at a point about 5 miles north of Shandon. Anomaly amplitudes and well data suggest that Salinian basement may be approximately 10,000 feet deep in the southern part of the low and perhaps 8,000 feet deep north of Shandon.

The broad northeast-trending gravity plateau near the junction of Shedd Canyon and Estrella River, 4 miles west-southwest of Shandon, is believed to represent a thinning of sedimentary rocks overlying an extension of basement rocks cropping out in the LaPanza Range southwest of the mapped area. The weak 2-mgal chevron-shaped high that is superposed on this gravity plateau and that follows the topographic lows of the Estrella River valley and Shedd Canyon results from the use of a Bouguer reduction density (2.67 g/cm^3) considerably larger than that of the Cenozoic rocks and deposits in this area. A similarly caused positive gravity flexure occurs over the valley of Cholame Creek, about 3 miles southwest of Cholame.

SUMMARY

Because of the great contrasts in lithology and structure of rocks on opposite sides of the San Andreas fault, as determined by geologic mapping and from well data, it is not surprising that gravity and magnetic features are quite dissimilar on opposite sides of the fault. The most conspicuous anomalies occur on the northeast side of the fault. They include (1) the largest gravity high within the mapped area, between Parkfield and Cholame, associated with Franciscan and Cretaceous miogeosynclinal rocks, (2) the elongate magnetic ridge and gravity trough at Table Mountain, presumably generated by a thick tabular serpentinite body dipping north-northeast, inferred to be the principal source of the serpentinite extrusion along this mountain, (3) the largest magnetic anomaly within the mapped area, which is also the largest anomaly known along the on-land part of the San Andreas fault, an elliptical high in an area of low gravity gradient, probably associated with a large deeply buried serpentine-rich body just northeast of the fault, and (4) a northwest-trending gravity low over the Kettleman Plain, probably reflecting a thickening of low-density Cenozoic sedimentary rocks near the axis of a major syncline.

The less conspicuous anomalies southwest of the San Andreas fault include (1) a local gravity high north of Red Hills, associated with an uplift of crystalline rocks in these hills on the northeast side of the San Juan fault, (2) a northwest-trending gravity gradient southeast of Red Hills, which suggests a buried basement fault or a steep subsurface contact between basement and sedimentary rocks from the San Juan fault southeastward to the San Andreas fault near the southern end of the quadrangle, (3) a discontinuous northwest-trending gravity trough east and north of Shandon, probably associated with low-density sedimentary rocks filling a depression of the basement surface near San Juan Creek, and (4) a broad northeast-trending gravity plateau west-southwest of Shandon, probably associated with a thinning of sedimentary rocks overlying a shallow basement surface that slopes from the extensive basement exposures of the La Panza Range southwest of the quadrangle.

The idealized cross sections of plate 4 pass through the areas of the largest gravity (*A–A′*) and magnetic (*B–B′*) anomalies within the mapped area. These cross sections illustrate the contrast in degree of deformation of upper crustal rocks on opposite sides of the San Andreas fault. Of special note in the sections is that, within the mapped area, typically magnetic serpentinite like that within the contact between Franciscan rocks and Cretaceous marine sedimentary rocks in parts of the northern California Coast Ranges (Irwin and Bath, 1962) is either absent or its volume is too small to be detected in the magnetic and gravity surveys.

REFERENCES

Bailey, E. H., and Everhart, D. L., 1964, Geology and quicksilver deposits of the New Almaden District, Santa Clara County, California: U.S. Geol. Survey Prof. Paper 360, 206 p.

Bailey, E. H., Irwin, W. P., and Jones, D. L., 1964, Franciscan and related rocks and their significance in the geology of western California: California Div. Mines and Geology Bull. 183, 177 p.

Bishop, C. C., and Chapman, R. H., 1967, Bouguer gravity map of California, Santa Cruz sheet: California Div. Mines and Geology, scale 1:250,000.

Bloxam, T. W., 1959, Glaucophane-schists and associated rocks near Valley Ford, California: Am. Jour. Sci., v. 257, no. 8, p. 95–112.

———1960, Jadeite-rocks and glaucophane schists from Angel Island, San Francisco Bay, California: Am. Jour. Sci., v. 258, no. 8, p. 555–573.

Borg, I. Y., 1956, Glaucophane schists and eclogites near Healdsburg, California: Geol. Soc. America Bull., v. 67, no. 2, pt. 1, p. 1563–1584.

Bott, M. H. P., 1960, The use of rapid digital computing methods for direct gravity interpretation of sedimentary basins: Royal Astron. Soc. Geophys. Jour., v. 3, p. 63–67.

Boyd, L. H., 1948, Gravity-meter survey of the Kettleman Hills–Lost Hills Trend, California, *in* Nettleton, L. L., ed., Geophysical case histories: Menasha, Wis., Soc. Exploration Geophysics, v. 1, p. 523–528.

Brown, R. D., Jr., Vedder, J. G., Wallace, R. E., Roth, E. F., Yerkes, R. F., Castle, R. O., Waananen, A. O., Page, R. W., and Eaton, J. P., 1967, The Parkfield-Cholame, California, earthquakes of June–August 1966—Surface geologic effects, water-resources aspects, and preliminary seismic data: U.S. Geol. Survey Prof. Paper 579, 66 p.

Burch, S. H., 1965, Tectonic emplacement of the Burro Mountain ultramafic body, southern Santa Lucia Range, California: Palo Alto, Calif., Stanford Univ., Ph. D. thesis, 159 p.

———1971, Complete Bouguer gravity and generalized geology of the Cape San Martin, Bryson, Piedras Blancas, and San Simeon quadrangles, California: U.S. Geol. Survey Prof. Paper 646–A, p. A1–A12.

Burch, S. H., and Durham, D. L., 1970, Complete Bouguer gravity and general geologic map of the Bradley, San Miguel, Adelaida, and Paso Robles quadrangles, California: U.S. Geol. Survey Prof. Paper 646–B, p. B1–B14.

Burch, S. H., Grannell, R. B., and Hanna, W. F., 1971, Bouguer gravity map of California, San Luis Obispo sheet: California Div. Mines and Geology, map, scale 1:250,000.

Burford, R. O., 1966, Strain analysis across the San Andreas fault and Coast Ranges of California: Acad. Sci. Fennicae Annales, Series A. III, Geologica-Geographica no. 90, p. 99–110.

Byerly, P. E., 1966, Interpretations of gravity data from the central Coast Ranges and San Joaquin Valley, California: Geol. Soc. America Bull., v. 77, no. 1, p. 83–94.

Chapman, R. H., 1966, The California Division of Mines and Geology gravity base station network: California Div. Mines and Geology Spec. Rept. 90, 49 p.

Clement, W. G., 1965, Complete Bouguer gravity map of the northern part of the San Francisco Bay area and its geologic interpretation: U.S. Geol. Survey Geophys. Inv. Map GP–468. scale 1:125,000.

Compton, R. R., 1966, Granitic and metamorphic rocks of the Salinian block, California Coast Ranges: California Div. Mines and Geology Bull. 190, p. 277–287.

Crowell, J. C., 1962, Displacement along the San Andreas fault, California: Geol. Soc. America Spec. Paper 71, 61 p.

Dibblee, T. W., Jr., 1966, Evidence for cumulative offset on the San Andreas fault in central and northern California *in* Bailey, E. H., ed., Geology of northern California: California Div. Mines and Geology Bull. 190, p. 375–384.

———1972, Stratigraphy of the southern Coast Ranges near the San Andreas fault from Cholame to Maricopa, California: U.S. Geol. Survey Prof. Paper 764. (In press.)

Dickinson, W. R., 1966a, Table Mountain serpentinite extrusion in California Coast Ranges: Geol. Soc. America Bull., v. 77, no. 5, p. 451–471.

———1966b, Structural relationships of the San Andreas fault system, Cholame Valley and Castle Mountain Range, California: Geol. Soc. America Bull., v. 77, no. 7, p. 707–726.

Dickinson, W. R., and Grantz, Arthur, eds., 1968, Proceedings of conference on geologic problems of San Andreas fault system: Stanford Univ. Pubs. Geol. Sci., v. 11, 374 p.

DuBois, R. L., 1963, Remanent, induced, and total magnetism of a suite of serpentine specimens from the Sierra Nevada, California: Jour. Geophys. Research, v. 68, no. 1, p. 267–278.

Eaton, J. P., 1968, Spatial distribution of aftershocks of the June 27, 1966, Parkfield-Cholame earthquake in the San Andreas fault zone *in* Dickinson, W. R., and Grantz, Arthur, eds., Proceedings of conference on geologic problems of San Andreas fault system: Stanford Univ. Pubs. Geol. Sci., v. 11, p. 84.

Eckel, E. B., and Meyers, W. B., 1946, Quicksilver deposits of the New Idria district, San Benito and Fresno counties, California: California Jour. Mines and Geology, v. 42, p. 81–124.

Evernden, J. F., Curtis, G. H., Savage, D. E., and James, G. T., 1964, Potassium-argon dates and the Cenozoic mammalian geochronology of North America: Am. Jour. Sci., v. 262, no. 2, p. 145–198.

Galehouse, J. S., 1967, Provenance and paleocurrents of the Paso Robles Formation, California: Geol. Soc. America Bull., v. 78, p. 951–978.

Griscom, Andrew, 1966, Magnetic data and regional structure in northern California *in* Bailey, E. H., ed, Geology of northern California: California Div. Mines and Geology Bull. 190, p. 407–417.

Grommé, C. S., and Gluskoter, H. J., 1965, Remanent magnetization of spilite and diabase in the Franciscan Formation, western Marin County, California: Jour. Geology, v. 73, p. 74–94.

Hanna, W. F., 1968a, Aeromagnetic and gravity reconnaissance over the central part of the San Andreas fault [abs.] *in* Dickinson, W. R., and Grantz, Arthur, eds., Proceedings of conference on geologic problems of San Andreas fault system: Stanford Univ. Pubs. Geol. Sci., v. 11, p. 214–215.

———1968b, Preliminary analysis of an induction-type apparatus for measuring magnetic susceptibility [abs.]: Am. Geophys. Union Trans., v. 49, no. 4, p. 673.

Hanna, W. F., Brown, R. D., Ross, D. C., and Griscom, Andrew, 1972, Aeromagnetic reconnaissance along the San Andreas fault between San Francisco and San Bernardino, California: U.S. Geol. Survey Geophys. Inv. Map GP–815, scale 1:250,000.

Hanna, W. F., and Burch, S. H., 1968, Anomalous gravity and magnetic fields along the San Andreas fault near Cholame, California [abs.]: Am. Geophys. Union Trans., v. 49, no. 4, p. 668.

Hay, E. A., 1963, Age and relationships of the Gold Hill pluton, Cholame Valley, California, *in* Guidebook to the geology of Salinas Valley and the San Andreas fault: Am. Assoc. Petroleum Geologists–Soc. Econ. Paleontologists and Mineralogists, Pacific Sec., Ann. Spring Field Trip, 1963, p. 113–115.

Henderson, R. G., and Zietz, Isidore, 1957, Graphical calculation of total intensity anomalies of three-dimensional bodies; Geophysics, v. 22, no. 4, p. 887–904.

Hill, M. L., and Dibblee, T. W., Jr., 1953, San Andreas, Garlock and Big Pine faults, California, a study of the character, history and tectonic signficance of their displacements: Geol. Soc. America Bull., v. 64, no. 4, p. 443–458.

Howard, J. H., 1968, Recent deformation of the Cholame and Taft-Maricopa areas, California, *in* Dickinson, W. R., and Grantz, Arthur, eds., Proceedings of conference on geologic problems of San Andreas fault system: Stanford Univ. Pubs. Geol. Sci., v. 11, p. 94–108.

Irwin, W. P., and Bath, G. D., 1962, Magnetic anomalies and ultramafic rock in northern California *in* Geological Survey research 1962: U.S. Geol. Survey Prof. Paper 450–B, p. B65–B67.

Jennings, C. W., and Strand, R. G., 1958, Geologic map of California, Olaf P. Jenkins edition, Santa Cruz Sheet: California Div. Mines and Geology, scale 1:250,000.

Marsh, O. T., 1960, Geology of the Orchard Peak area, California: California Div. Mines Spec. Rept. 62, 42 p.

Plouff, Donald, 1966, Digital terrain corrections based on geographic coordinates [abs.]: Geophysics, v. 31, no. 6, p. 1208.

Reed, R. D., 1933, Geology of California: Tulsa, Okla., Am. Assoc. Petroleum Geologists, 355 p.

Ross, D. C., 1970, Quartz gabbro and anorthositic gabbro: Markers of offset along the San Andreas fault in the California Coast Ranges: Geol. Soc. America Bull., v. 81, no. 12, p. 3647–3661.

Saad, A. H., 1968, Magnetic properties of ultramafic rocks from Red Mountain, California: Palo Alto, Calif., Stanford Univ., Ph.D. thesis, 59 p.

Swick, C. H., 1942, Pendulum gravity measurements and isostatic reductions: U.S. Coast and Geodetic Survey Spec. Pub. 232, 82 p.

Talwani, Manik, and Ewing, Maurice, 1960, Rapid computation of gravitational attraction of three-dimensional bodies of arbitrary shape: Geophysics, v. 25, no. 1, p. 203–225.

Talwani, Manik, Worzel, J. L., and Landisman, Mark, 1959, Rapid gravity computations for two-dimensional bodies with application to the Mendocino submarine fracture zone: Jour. Geophys. Research, v. 64, no. 1, p. 49–59.

Thompson, G. A., and Talwani, Manik, 1964, Crustal structure from Pacific basin to central Nevada: Jour. Geophys. Research, v. 69, no. 22, p. 4813–4837.

Wentworth, C. M., 1968, Upper Cretaceous and lower Tertiary strata near Gualala, California, *in* Dickinson, W. R., and Grantz, Arthur, eds., Proceedings of conference on geologic problems of San Andreas fault system: Stanford Univ. Pubs. Geol. Sci., v. 11, p. 130–143.

Woodring, W. P., Stewart, Ralph, and Richards, R. W., 1940, Geology of the Kettleman Hills Oil Field, California: U.S. Geol. Survey Prof. Paper 195, p. 27–53.

469-845 O - 73 - 3